NATIONAL ADVISORY COMMITTEE FOR AERONAUTICS

TECHNICAL NOTE 2321

ANALYSIS OF TEMPERATURE DISTRIBUTION IN LIQUID-COOLED TURBINE BLADES

By John N. B. Livingood and W. Byron Brown

Lewis Flight Propulsion Laboratory
Cleveland, Ohio

Washington
April 1951

NATIONAL ADVISORY COMMITTEE FOR AERONAUTICS

TECHNICAL NOTE 2321

ANALYSIS OF TEMPERATURE DISTRIBUTION IN LIQUID-COOLED TURBINE BLADES

By John N. B. Livingood and W. Byron Brown

SUMMARY

The temperature distribution in liquid-cooled turbine blades determines the amount of cooling required to reduce the blade temperature to permissible values at specified locations. This report presents analytical methods for computing temperature distributions in liquid-cooled turbine blades, or in simplified shapes used to approximate sections of the blades.

The individual analyses are first presented in terms of their mathematical development. By means of numerical examples, comparisons are made between simplified and more complete solutions and the effects of several variables are examined. Nondimensional charts to simplify some temperature-distribution calculations are also given.

It was found that for blade materials having low thermal conductivities (corresponding to blade materials in current use) a one-dimensional spanwise temperature-distribution equation is applicable near a coolant passage. The cooled part of the blade, irrespective of blade length, was found to remain at a determinable uniform temperature, called the prevalent blade temperature. The prevalent blade temperature increased about 150° F for an increase in the difference between the effective gas temperature and the coolant temperature of 1000° F for a range of effective gas temperature from 2000° to 5000° F.

In cases where rim cooling is insignificant, it was found that a one-dimensional chordwise temperature-distribution equation was sufficiently near the relaxation solution for the actual blade shape for a first-order approximation.

INTRODUCTION

A limitation on design and performance of aircraft gas-turbine power plants is the strength of the turbine materials, which decreases as temperature increases. This limitation may be greatly alleviated, even when nonstrategic materials are used, by the application of turbine cooling. An extensive study of both liquid and air cooling of turbine blades has been carried out at the NACA Lewis laboratory since 1945.

The temperature distribution in a turbine blade determines the amount of cooling required to reduce the blade temperature to permissible values at specified locations. Analytical studies have been conducted to predict temperature distributions in cooled turbine blades. A summary of the analytical methods developed for calculating spanwise temperature distributions for three types of air-cooled turbine blade is presented in reference 1. The present report summarizes the analytical methods developed for calculating temperature distributions in liquid-cooled turbine blades. Parts of these analyses are presented in references 2 and 3.

Because the calculation of a generalized three-dimensional temperature distribution through a liquid-cooled turbine blade is too tedious to be of practical value and because some knowledge of the distribution in a radial direction is necessary, the first investigation presented herein is limited to a one-dimensional spanwise distribution. This distribution, however, is only valid in the immediate vicinity of the coolant passages. In order to study more accurately the temperature distribution in the trailing section of the blade, a three-dimensional solution is determined for a rectangular parallelepiped used to approximate a blade trailing section. This solution serves to determine the importance of blade thermal conductivity and of distance from the coolant passage. Because numerical calculations for a rectangular parallelepiped produce a constant spanwise temperature in the region of the blade beyond the influence of rim cooling (that is, in the region of the blade unaffected by conduction to the rim), one-dimensional chordwise temperature distributions are then calculated for shapes approximating various parts of a blade cross section; these investigations are valid for the part of the blade beyond the influence of rim cooling. Finally, a two-dimensional temperature distribution through the cross section of an actual blade shape is obtained in order to determine the accuracy of the previously determined approximate solutions and to study the effect on temperature distribution of a peripheral variation of gas-to-blade heat-transfer coefficient.

Numerical examples based on coefficients available from unclassified sources are included.

METHODS OF ANALYSIS

One-dimensional spanwise, three-dimensional, one-dimensional chordwise, and two-dimensional chordwise temperature-distribution equations for liquid-cooled turbine blades or for simplified shapes used to approximate sections of liquid-cooled turbine blades are presented.

For simplicity in presentation, the individual analyses are first formulated in terms of the mathematical methods. The comparative applicabilities of the methods of analysis are established in later sections of the report.

For all the analyses presented, the following conditions are assumed:

(1) The coolant temperature is constant at the average temperature of the coolant, or the coolant forms a constant-temperature reservoir. This assumption is valid when the change in coolant temperature is small in comparison with the temperature difference between the gas and the coolant.

(2) The blade-to-coolant heat-transfer coefficient is constant.

(3) The thermal conductivity of the blade is constant.

(4) The effective gas temperature at all parts of the blade is the same.

(5) Radiation effects are considered to be included in the heat-transfer coefficients. The following individual analyses are presented:

One-dimensional spanwise temperature distribution. - A one-dimensional spanwise calculation gives a radial temperature distribution valid in a part of the blade near a coolant passage. In this particular case, the radial temperature distribution is carried through the blade and through the turbine rotor. Heat transfer between the turbine rotor and the fluid on the outside of the rotor is assumed to take place and a constant value of gas-to-blade heat-transfer coefficient is assumed. For simplicity, a blade of constant cross-sectional area and perimeter is considered.

For blades with little taper, the method is applicable if average cross-sectional area and perimeter are considered. In general, however, a numerical solution is necessary for tapered blades.

Three-dimensional temperature distribution through simplified trailing section. - A three-dimensional temperature distribution for the trailing section of the blade is obtained by considering this part of the blade as a rectangular parallelepiped. The blade-root temperature is considered constant, the gas-to-blade heat-transfer coefficient is constant, and it is assumed that no heat flows across the median plane of the simplified blade section.

An approximate solution for tapered blades is obtainable by this method if the blade is considered in small sections, average values of cross-sectional area and perimeter are considered for each section, and appropriate compatability relations are satisfied.

One-dimensional chordwise temperature distributions through simplified shapes. - Rectangular and trapezoidal sections, concentric circle annuli, and sections between parallel plates are considered as the simplified shapes used to approximate parts of a turbine-blade cross section. The gas-to-blade heat-transfer coefficient is considered constant. For comparison purposes, the rectangular and trapezoidal sections are constructed so that lengths and areas are identical.

Two-dimensional chordwise temperature distribution. - Numerical two-dimensional temperature distributions through the cross section of an actual blade shape are determined. Constant and variable gas-to-blade heat-transfer coefficients are considered.

One-Dimensional Spanwise Temperature Distribution

The spanwise temperature-distribution equations for a liquid-cooled turbine, a section of which is shown in figure 1, are derived in reference 2 and are reproduced in appendix B. In this spanwise case, the investigation was extended from blade tip to rotor hub.

For convenience, the turbine was divided into four sections (fig. 1), and the temperature-distribution equations were obtained from heat balances for differential elements in each section. Inasmuch as chordwise conduction was neglected, the following equations, valid only in the neighborhood of the coolant passages, were obtained. For the uncooled section of the blade (fig. 1, section 1), it was found that

$$T_{B,1} = T_{g,e} - C_1 \cosh \mathscr{a}(x_1 + C_2) \tag{1}$$

where C_1 and C_2 are integration constants and

$$\mathscr{a} = \left(\frac{h_o l_o}{k_B A_{B,1}}\right)^{\frac{1}{2}}$$

(All symbols are defined in appendix A.) The value of C_2 is determined by use of the boundary condition at the blade tip (where heat enters by convection only).

$$-k_B A_{B,1} \left(\frac{dT_B}{dx_1}\right)_T = h_o A_{B,1} (T_{g,e} - T_{B,T})$$

or

$$\tanh \mathscr{A} C_2 = \frac{h_o}{k_B \mathscr{A}} = \left(\frac{h_o A_{B,1}}{l_o k_B}\right)^{\frac{1}{2}}$$

For the cooled section of the blade (fig. 1, section 2), it was found that

$$T_{B,2} = T_{B,p} - C_3 e^{\mathscr{B} x_2} - C_4 e^{-\mathscr{B} x_2} \tag{2}$$

where C_3 and C_4 are integration constants,

$$T_{B,p} = \frac{h_o l_o T_{g,e} + h_{i,2} l_{i,2} T_l}{h_o l_o + h_{i,2} l_{i,2}} \tag{2a}$$

and

$$\mathscr{B} = \left(\frac{h_o l_o + h_{i,2} l_{i,2}}{k_B A_{B,2}}\right)^{\frac{1}{2}}$$

The prevalent blade temperature $T_{B,p}$ is the temperature the blade would assume if no heat flows in or out of the blade ends.

For the rim section (fig. 1, section 3), with assumed constant area,

$$T_{rim} = \mathscr{G} + C_5 e^{\mathscr{E} x_3} + C_6 e^{-\mathscr{E} x_3} \tag{3}$$

where C_5 and C_6 are integration constants,

$$\mathscr{G} = \left[\frac{4\pi r_{3,av} h_a T_a + (h_{i,3} l_{i,3})_{av} T_l}{4\pi r_{3,av} h_a + (h_{i,3} l_{i,3})_{av}}\right]$$

$$\mathscr{E} = \left[\frac{4\pi r_{3,av} h_a + (h_{i,3} l_{i,3})_{av}}{k_{rim} A_{rim}}\right]^{\frac{1}{2}}$$

and T_a is the fluid temperature on the outside of the rotor and $(h_{i,3} l_{i,3})_{av}$ is the average of the values of $h_{i,3} l_{i,3}$ found for the blade coolant passages, the rim circumferential passages, and the radial passages through the rotor (fig. 1).

For the rotor section (fig. 1, section 4), with assumed constant strength,

$$T_R = \mathscr{J} + C_7 \cosh \mathscr{H} r \tag{4}$$

where C_7 is an integration constant, and where

$$\mathscr{J} = \frac{4\pi r_{4,av} h_a T_a + (h_{i,4} l_{i,4})_{av} T_l}{4\pi r_{4,av} h_a + (h_{i,4} l_{i,4})_{av}}$$

and

$$\mathscr{H} = \left[\frac{4\pi r_{4,av} h_a + (h_{i,4} l_{i,4})_{av}}{k_R A_R}\right]^{\frac{1}{2}}$$

Values of the six integration constants C_1, C_3, C_4, C_5, C_6, and C_7 are found by solving simultaneously the six equations resulting from equating temperatures and heat flows at the various junction points of the four sections of the turbine. (Subscripts α and β used after numerical subscripts designate the end nearest the blade tip and the end nearest the rotor hub of the sections to which the numerical subscripts refer, respectively.) At the junctions of sections 1 and 2,

$$T_{g,e} - C_1 \cosh \mathscr{A}(x_{1,\beta} + C_2) = T_{B,p} - C_3 e^{\mathscr{B} x_{2,\alpha}} - C_4 e^{-\mathscr{B} x_{2,\alpha}} \tag{5}$$

$$k_B A_{B,1,\beta} C_1 \mathscr{A} \sinh \mathscr{A}(x_{1,\beta} + C_2) = \mathscr{B} k_B A_{B,2,\alpha} \left(C_3 e^{\mathscr{B} x_{2,\alpha}} - C_4 e^{-\mathscr{B} x_{2,\alpha}}\right) +$$

$$h_{i,1}(A_{B,1,\beta} - A_{B,2,\alpha}) \left(T_{B,p} - C_3 e^{\mathscr{B} x_{2,\alpha}} - C_4 e^{-\mathscr{B} x_{2,\alpha}} - T_l\right) \tag{6}$$

Equation (6) equates the heat leaving section 1 to the sum of the heat entering the metal of section 2 and the heat entering the coolant at that part of the blade where the inlet and outlet passages are connected. An approximation in the procedure has been introduced at this point because a separate blade section for the part of the blade containing the connecting passage between inlet and outlet passages is not introduced. A numerical calculation showed that use of such a section would slightly decrease the temperature at the blade tip.

At the junction of sections 2 and 3,

$$T_{B,p} - C_3 e^{\mathscr{B} x_{2,\beta}} - C_4 e^{-\mathscr{B} x_{2,\beta}} = \mathscr{G} + C_5 e^{\mathscr{E} x_{3,\alpha}} + C_6 e^{-\mathscr{E} x_{3,\alpha}} \tag{7}$$

$$k_B A_{B,2} \mathscr{B}\left(C_3 e^{\mathscr{B} x_{2,\beta}} - C_4 e^{-\mathscr{B} x_{2,\beta}}\right) +$$

$$\frac{A_{rim} - ZA_{B,2}}{ZA_{B,2}} h_o A_{B,2} \left(T_{g,e} - T_{B,p} + C_3 e^{\mathscr{B} x_{2,\beta}} + C_4 e^{-\mathscr{B} x_{2,\beta}}\right)$$

$$= \mathscr{E} k_B A_{B,2} \frac{A_{rim}}{ZA_{B,2}} \left(C_6 e^{-\mathscr{E} x_{3,\alpha}} - C_5 e^{\mathscr{E} x_{3,\alpha}}\right) \tag{8}$$

Equation (8) equates the sum of the heat leaving section 2 and that entering section 3 directly from the hot gases to the total heat entering section 3.

At the junctions of sections 3 and 4,

$$\mathscr{G} + C_5 e^{\mathscr{E} x_{3,\beta}} + C_6 e^{-\mathscr{E} x_{3,\beta}} = \mathscr{J} + C_7 \cosh \mathscr{H} r_\alpha \tag{9}$$

$$k_B \mathscr{E}\left(-C_5 e^{\mathscr{E} x_{3,\beta}} + C_6 e^{-\mathscr{E} x_{3,\beta}}\right) = \frac{A_R}{A_{rim}} k_B \mathscr{H} C_7 \sinh \mathscr{H} r_\alpha \tag{10}$$

Three-Dimensional Temperature Distribution through Simplified Trailing Section

The spanwise temperature-distribution equations previously presented are valid only in the neighborhood of the coolant passages. Most

currently used turbine blades are so shaped that coolant passages cannot be located near the trailing edge. Because of the impossibility of placing reasonably large coolant passages near the trailing edges of conventional turbine blades and because the trailing sections seem most likely to be the hottest parts of the blade, other detailed studies were made of temperature distributions. The first study was devoted to approximating the trailing section by a rectangular parallelepiped and to determining the three-dimensional temperature distribution through this parallelepiped (fig. 2).

The median plane of the rectangular parallelepiped was chosen as the plane $z = 0$, and symmetry was assumed about this plane (no heat flow was assumed to cross this plane, as previously stated). Boundary conditions at the blade trailing edge and blade tip were simplified by assuming the blade width and blade length to be extended by a distance equal to one-half the blade thickness. In figure 3, the edge MN at temperature T gained some heat from the gas stream. The extended surfaces NO and MP were at nearly the same temperature T and no heat entered the edge OP; these surfaces therefore gained practically the same amount of heat as the actual exposed edge. The validity of this approximation is discussed in reference 4 (pp. 216 and 217). Distances increased by $\tau/2$ are denoted by primes.

The derivation of the three-dimensional temperature distribution, originally derived in reference 3, is reproduced in appendix C. The differential equation, in final form, for the temperature distribution is found to be

$$\frac{\partial^2\theta}{\partial x'^2} + \frac{\partial^2\theta}{\partial y'^2} + \frac{\partial^2\theta}{\partial z^2} = 0 \tag{11}$$

where x' and y' denote x and y increased by $\tau/2$, respectively. A solution of equation (11) satisfying the boundary conditions at $x' = y' = z = 0$ is

$$\theta = \sum_{m=1}^{\infty}\sum_{n=1}^{\infty}\left(\mathscr{K}_{m,n}\cos\mathscr{L}_n x' \cosh\mathscr{M}_{m,n}y' \cos\mathscr{N}_m z + \mathscr{O}_{m,n}\cosh\mathscr{P}_{m,n}x' \cos\mathscr{Q}_n y' \cos\mathscr{N}_m z\right) \tag{12}$$

where $\mathscr{K}$, $\mathscr{L}$, $\mathscr{M}$, $\mathscr{N}$, $\mathscr{O}$, $\mathscr{P}$, and $\mathscr{Q}$ are constants. Relations among the constants are

$$\left.\begin{aligned} \mathscr{M}_{m,n}^{2} &= \mathscr{N}_{m}^{2} + \mathscr{L}_{n}^{2} \\ \mathscr{P}_{m,n}^{2} &= \mathscr{N}_{m}^{2} + \mathscr{Q}_{n}^{2} \end{aligned}\right\} \quad m,n = 1,2,3, \ldots \tag{13}$$

Values of $\mathscr{K}_{m,n}$ and $\mathscr{O}_{m,n}$ are given by the relations

$$\mathscr{K}_{m,n} = \frac{(-1)^{n-1}}{\pi(2n-1)} \frac{\sin \mathscr{N}_m \frac{\tau}{2}}{\mathscr{N}_m \frac{\tau}{2}} \frac{8h_i(T_{g,e}-T_l)}{\left(1 + \frac{\sin 2\mathscr{N}_m \frac{\tau}{2}}{2\mathscr{N}_m \frac{\tau}{2}}\right)} \left(\frac{1}{k_B \mathscr{M}_{m,n} \sinh \mathscr{M}_{m,n} j' + h_i \cosh \mathscr{M}_{m,n} j'}\right) \tag{14}$$

and

$$\mathscr{O}_{m,n} = \frac{\sin \mathscr{Q}_n j'}{\mathscr{Q}_n j'} \frac{4(T_{g,e}-T_{B,r})}{\left(1 + \frac{\sin 2\mathscr{Q}_n j'}{2\mathscr{Q}_n j'}\right)} \frac{\sin \mathscr{N}_m \frac{\tau}{2}}{\mathscr{N}_m \frac{\tau}{2}} \frac{1}{\left(1 + \frac{\sin 2\mathscr{N}_m \frac{\tau}{2}}{2\mathscr{N}_m \frac{\tau}{2}}\right)} \frac{1}{\cosh \mathscr{P}_{m,n} b'} \tag{15}$$

Application of the boundary conditions at $x' = b'$, $y' = j'$, and $z = \tau/2$ lead to the following methods of evaluating $\mathscr{L}$, $\mathscr{Q}$, and $\mathscr{N}$, respectively:

$$\mathscr{L}_n = \left(n - \frac{1}{2}\right) \frac{\pi}{b'} \tag{16}$$

$$\tan \mathscr{Q}_n j' = \frac{h_i}{k_B \mathscr{Q}_n} = \frac{\frac{h_i j'}{k_B}}{\mathscr{Q}_n j'} \tag{17}$$

and

$$\tan \mathscr{N}_m \frac{\tau}{2} = \frac{h_o}{k_B \mathscr{N}_m} = \frac{\frac{h_o \tau}{2k_B}}{\frac{\mathscr{N}_m \tau}{2}} \tag{18}$$

It is at once obvious that from equation (16) many values of $\mathscr{L}_n$ result. Because of the periodicity of the tangent function, equations (17) and (18) likewise have many solutions.

Values for all the constants in equation (12) can thus be found and the temperature can now be computed at any point in the rectangular parallelepiped. In reference 3, appendix B, it is shown that sufficiently accurate results can be obtained by using $m = 1$ only.

One-Dimensional Chordwise Temperature Distributions through Simplified Shapes

Because the spanwise temperature distributions are valid only in the neighborhood of the coolant passages and because the three-dimensional approximate solution resulted in a constant spanwise blade temperature in the part of the blade beyond the influence of rim cooling, one-dimensional chordwise temperature distributions were determined for sections of a liquid-cooled turbine blade that can be approximated by simple shapes (fig. 4). Rectangular and trapezoidal approximations for blade trailing sections were considered. Trapezoidal sections may also be used to approximate the leading section in some blades. In addition, analyses were made for leading sections approximated by concentric circle annuli and for the sections of blades with very little metal between blade outer surface and coolant passages approximated as regions between parallel plates. The temperature distributions through these simplified shapes, derived in appendix D and valid in regions beyond the influence of rim cooling, follow.

Rectangular trailing section of blade removed from influence of rim cooling. - For a blade trailing section approximated by a rectangle (fig. 4(a)) the temperature-distribution equation is

$$\theta = \frac{\frac{h_i}{k_B}(T_{g,e} - T_l) \cosh(\varphi y')}{\varphi \sinh \varphi j' + \frac{h_i}{k_B} \cosh \varphi j'} \tag{19}$$

where

$$\theta = T_{g,e} - T_B$$

and

$$\varphi = \left(\frac{2h_o}{k_B \tau}\right)^{\frac{1}{2}}$$

Trapezoidal trailing section of blade removed from influence of rim cooling. - For a trapezoidal approximation to the blade trailing section (fig. 4(b)), the temperature distribution is

$$\theta = \frac{\frac{h_i \zeta_2}{2K^2 k_B}(T_{g,e} - T_l)\left[H_1(i\zeta_1)J_o(i\zeta) + iJ_1(i\zeta_1)iH_o(i\zeta)\right]}{\left[iJ_1(i\zeta_1)H_1(i\zeta_2)\right] - \left[H_1(i\zeta_1)iJ_1(i\zeta_2)\right] + \frac{h_i \zeta_2}{2K^2 k_B}\Gamma} \tag{20}$$

where

$$\zeta = 2K\left[y' + \frac{\tau_1(1 - \tan\psi)}{2\tan\psi}\right]^{\frac{1}{2}}$$

$$\zeta_1 = 2K\left[\frac{\tau_1(1 - \tan\psi)}{2\tan\psi}\right]^{\frac{1}{2}}$$

$$\zeta_2 = 2K\left[j' + \frac{\tau_1(1 - \tan\psi)}{2\tan\psi}\right]^{\frac{1}{2}}$$

$$K = \left(\frac{h_o}{k_B \sin\psi}\right)^{\frac{1}{2}}$$

$$\psi = \tan^{-1}\frac{\tau_2 - \tau_1}{2j}$$

$$\Gamma = H_1(i\zeta_1)J_o(i\zeta_2) + iJ_1(i\zeta_1)iH_o(i\zeta_2)$$

and J_o, iJ_1, H_o, and iH_1 are Bessel functions. For a wedge-shaped section the temperature-distribution equation (20) reduces to

$$\theta = \frac{\frac{h_i \zeta_2}{2K^2 k_B}(T_{g,e}-T_l)J_o(i\zeta)}{\frac{h_i \zeta_2}{2K^2 k_B} J_o(i\zeta_2) - iJ_1(i\zeta_2)} \tag{21}$$

Concentric-circle-annulus approximation for blade leading section. - The equations expressing the blade-metal temperature at the coolant passage wall $T_{B,i}$, at the leading edge of the blade $T_{B,o}$, and at any point in the annulus T_B are found to be (fig. 4(c))

$$T_{B,i} = T_l + \left\{\left[\frac{2k_B}{D_i h_i \log_e\left(\frac{D_o}{D_i}\right)}\right]\right\}(T_{B,o}-T_{B,i}) \tag{22}$$

$$T_{B,o} = T_{g,e} - \left\{\left[\frac{2k_B}{D_o h_o \log_e\left(\frac{D_o}{D_i}\right)}\right]\right\}(T_{B,o}-T_{B,i}) \tag{23}$$

and

$$T_B = T_{B,i} + \frac{\log_e\left(\frac{D}{D_i}\right)}{\log_e\left(\frac{D_o}{D_i}\right)}(T_{B,o}-T_{B,i}) \tag{24}$$

where

$$T_{B,o}-T_{B,i} = \frac{T_{g,e}-T_l}{1 + \frac{k_B}{\log_e\left(\frac{D_o}{D_i}\right)}\left(\frac{2}{D_o h_o} + \frac{2}{D_i h_i}\right)} \tag{25}$$

Section of blade approximated by parallel plates. - The equations expressing the blade-metal temperatures at the coolant-passage wall (fig. 4(d)) $T_{B,i}$ and at the blade outer edge $T_{B,o}$ are

$$T_{B,i} = \frac{T_l + \left(\frac{k_B}{\sigma h_o h_i}\right)(h_o T_{g,e} + h_i T_l)}{1 + \left(\frac{k_B}{\sigma h_o h_i}\right)(h_o + h_i)} \tag{26}$$

and

$$T_{B,o} = \frac{T_{g,e} + \left(\frac{k_B}{\sigma h_o h_i}\right)(h_o T_{g,e} + h_i T_l)}{1 + \left(\frac{k_B}{\sigma h_o h_i}\right)(h_o + h_i)} \tag{27}$$

where σ is the distance between the parallel plates.

Two-Dimensional Chordwise Temperature Distribution

The temperature at any point on the blade cross section may be found by solving the Laplace differential equation given in terms of the temperature difference θ

$$\frac{\partial^2 \theta}{\partial X^2} + \frac{\partial^2 \theta}{\partial Y^2} = 0 \tag{28}$$

where X and Y are the Cartesian coordinates in the blade cross section. The boundary conditions, expressed in terms of the partial derivative of θ in the direction normal to the boundary are

$$\frac{\partial \theta}{\partial n} = \frac{h_o}{k_B}\theta \tag{29}$$

at the outer boundary and

$$\frac{\partial \theta}{\partial n} = \frac{h_i}{k_B}(T_{g,e} - T_l - \theta) \tag{30}$$

at the coolant-passage boundary.

A closed solution to equation (28) cannot be obtained because of the impossibility of applying the given boundary conditions along the odd-shaped boundary of a turbine blade (fig. 5). A numerical solution is available, however, by application of the relaxation method (reference 5). A sketch of the blade cross section is covered by a network

of points (a square network was chosen). Large net spacings are recommended at first, and the insertion of additional net points may be made at any time during the solution, thus permitting the use of a final network of any desired size. Temperature estimates for the net points can be obtained from the solutions of the chordwise blade-temperature-distribution equations for approximate shapes previously presented and from application of the boundary conditions given by equations (29) and (30). Residuals, which may be considered as interior heat sinks, can then be calculated at each net point whose immediately neighboring points remain within the boundary from the relation

$$\bar{Q}_0 = \theta_1+\theta_2+\theta_3+\theta_4-4\theta_0 \tag{31}$$

where the subscript zero denotes a point in the blade cross section and subscripts 1, 2, 3, and 4 denote the points in the square surrounding the point with zero subscript.

The object of the relaxation is to reduce the values of $\bar{Q}$ to zero, or as close to zero as possible. When the relaxation equation (31) is employed, the following procedure is used. A change in θ_0 alters $\bar{Q}_1$, $\bar{Q}_2$, $\bar{Q}_3$, $\bar{Q}_4$ by the same change and $\bar{Q}_0$ by minus four times this change, all other values of θ remaining fixed.

Equation (31) is the finite-difference equation corresponding to the partial differential equation (28). For net points some of whose immediately neighboring points lie outside the boundary, equation (31) must be modified. For example, if point 1 lies outside the boundary and point 5 is the boundary point between 0 and 1, the following equation applies:

$$\bar{Q}_0 = \theta_2+\theta_3+\theta_4 + \frac{\theta_5}{d} - \left(3 + \frac{1}{d}\right)\theta_0 \tag{32}$$

where d is the ratio of the distance between points 0 and 5 to the net spacing.

Corresponding changes in the values of $\bar{Q}$ result from the use of equation (32). No harm is done by overestimating the final values of θ, as successive calculations will establish them again. Continued relaxation eventually reduces all the residuals as desired and the blade temperatures can finally be obtained from the definition of θ,

$$\theta = T_{g,e}-T_B$$

APPLICATION OF ANALYSIS

Typical numerical examples for a sample blade are presented to illustrate temperature trends and to determine the effects of various factors on the temperature distributions in a liquid-cooled turbine blade. A turbine blade whose external shape is similar to that of the rotor-root section of a conventional gas-turbine design was selected as the sample blade. Two 0.25-inch-diameter coolant passages were assumed in the blade (fig. 5), connected near the blade tip by a cross-over passage, and the cooling was assumed to occur through forced convection. No allowance was made in these calculations for the effects of free-convection currents that might be present. A gas flow of 55 pounds per second (equivalent to a mass velocity of about 58 lb/(sec)(sq ft)) and a coolant flow of 7 pounds per minute per blade were assumed (to insure turbulent flow and to remove the dependence of the blade-to-coolant heat-transfer coefficient on the length-to-diameter ratio of the coolant passage).

For the one-dimensional spanwise case, in which the cooling was carried to the rotor hub, two 0.25-inch-diameter coolant passages running circumferentially through the rim and ten 0.50-inch-diameter coolant passages running radially through the rotor were assumed (fig. 1). For this case, water, ethylene glycol, and kerosene were all considered as possible coolants. Other calculations were made only for water as the coolant because of its superiority over the other coolants considered.

Blade-to-coolant average heat-transfer coefficients were calculated by use of formulas presented in reference 6, page 168 for turbulent flow and page 190 for laminar flow (for ethylene glycol only). Gas-to-blade average heat-transfer coefficients were calculated by use of formulas given on page 236 of reference 6. The following coefficients were used in the analysis:

Outside heat-transfer coefficient, h_o	
Btu/(hr)(sq ft)($^\circ$F)	222
Btu/(sec)(sq ft)($^\circ$F)	0.06167
Inside heat-transfer coefficient, $h_{i,2}$	
Water, Btu/(hr)(sq ft)($^\circ$F)	2370
Btu/(sec)(sq ft)($^\circ$F)	0.6583
Ethylene glycol, Btu/(hr)(sq ft)($^\circ$F)	649
Btu/(sec)(sq ft)($^\circ$F)	0.1803
Kerosene, Btu/(hr)(sq ft)($^\circ$F)	510
Btu/(sec)(sq ft)($^\circ$F)	0.1417

Other numerical values used in the calculations were (figs. 1 and 4):

Effective gas temperature, $T_{g,e}$, $^{\circ}F$	2000 - 5000
Average coolant temperature, T_l, $^{\circ}F$	200
Number of blades, Z	55
Area of blade cross section 1, A_1, sq ft	0.00198
Area of blade cross section 2, A_2, sq ft	0.0013
Area of cross section 3, A_3, sq ft	0.312
Area of cross section 4, A_4, sq ft	0.236
Blade outside perimeter, l_o, ft	0.2542
Blade inside perimeter, $l_{i,2}$, ft	0.131
Average radial distance, section 3, $r_{3,av}$, ft	0.4917
Average radial distance, section 4, $r_{4,av}$, ft	0.3333
Length of chordwise trailing section, j, ft	0.050
Length of spanwise trailing section, b, ft	0.3333
Thickness of trapezoid at coolant passage, τ_2, ft	0.021
Thickness of trapezoid at trailing edge, τ_1, ft	0.003
Thickness of rectangle, τ, ft	0.010
Temperature at blade root, T_r, $^{\circ}F$	330
Thermal conductivity, k_B	
Btu/(hr)(ft)($^{\circ}F$)	15 - 210
Btu/(sec)(ft)($^{\circ}F$)	0.00417 - 0.0583
Cooling-air (in contact with rotor) temperature, T_a, $^{\circ}F$	0
Heat-transfer coefficient between cooling air and rotor, h_a	
Btu/(hr)(sq ft)($^{\circ}F$)	30
Btu/(sec)(sq ft)($^{\circ}F$)	0.00874
Average value in section 3 of $l_{i,3}h_{i,3}$	
Water, Btu/(hr)(ft)($^{\circ}F$)	30,360
Btu/(sec)(ft)($^{\circ}F$)	8.433
Ethylene glycol, Btu/(hr)(ft)($^{\circ}F$)	8305
Btu/(sec)(ft)($^{\circ}F$)	2.307
Kerosene, Btu/(hr)(ft)($^{\circ}F$)	6533
Btu/(sec)(ft)($^{\circ}F$)	1.815
Average value in section 4 of $l_{i,4}h_{i,4}$	
Water, Btu/(hr)(ft)($^{\circ}F$)	6107
Btu/(sec)(ft)($^{\circ}F$)	1.696
Ethylene glycol, Btu/(hr)(ft)($^{\circ}F$)	1656
Btu/(sec)(ft)($^{\circ}F$)	0.460
Kerosene, Btu/(hr)(ft)($^{\circ}F$)	1318
Btu/(sec)(ft)($^{\circ}F$)	0.366

One-Dimensional Spanwise Temperature Distribution

The constants of integration were found by solving equations (5) to (10) for the specific examples stated; a blade thermal conductivity of 15 Btu/(hr)(ft)($^{\circ}$F) was used. Blade coolant passages extending to within 1/16 inch of the blade tip were considered in blades with spans ranging from $1\frac{1}{16}$ to $4\frac{1}{16}$ inches, with water as coolant, and for effective gas temperature ranging from 2000° to 5000° F in order to study the effect of blade length on the temperature distribution. The temperature distributions were determined, by use of the calculated integration constants, from equations (1) to (4) and are shown in figure 6. The general trend shown is a nearly constant temperature about equal to the coolant temperature through the rotor, a sharp temperature increase through the rim and the base of the blade, a nearly constant temperature (called the prevalent blade temperature) through the liquid-cooled part of the blade, and another sharp temperature increase to a value approaching the effective gas temperature in the uncooled part of the blade. From figure 6, it can readily be seen that the same prevalent blade temperature prevails through blades of various lengths cooled to within 1/16 inch of the blade tip.

In order to study the effect of coolant-passage length on the temperature distribution, other calculations were made, with water as coolant and for an effective gas temperature of 2000° F, for a $4\frac{1}{16}$ inch blade span but with blade coolant passages of various lengths. The calculations, again determined by use of equations (1) to (4), are plotted in figure 7; for short coolant passages high-temperature gradients exist throughout the blade whereas for long coolant passages practically no temperature gradient exists throughout most of the blades.

Calculations were also made for the same blades with 4-inch coolant passages and for an effective gas temperature of 2000° F with water, ethylene glycol, and kerosene considered as possible coolants. These results showing the effect of various coolants on temperature distribution are given in figure 8. For an effective gas temperature of 2000° F and a coolant flow of 7 pounds per minute per blade, the prevalent blade temperature in degrees Fahrenheit is about one fourth, two fifths, and one half of the effective gas temperature for water, ethylene glycol, and kerosene coolants, respectively. The consideration of cooling air on the outside of the rotor accounts for the rotor temperature being less than the coolant temperature.

Finally, for the spanwise case, figure 9 shows the variation of coolant flow on prevalent blade temperature. The prevalent blade temperature decreases with increasing coolant flow; the rate of this

decrease diminishes as the coolant flow increases. It can be seen that the cooling effectiveness, defined as $(T_{g,e}-T_B)/(T_{g,e}-T_l)$, changes from 0.68 to 0.91 for water as the coolant flow is increased from 2 to 16 pounds per minute per blade. The superiority of water is apparent.

Three-Dimensional Temperature Distribution through Simplified Trailing Section

A three-dimensional temperature distribution in a turbine-blade trailing section approximated by a rectangular parallelepiped (fig. 2) was determined by use of equation (12) (approximated by use of $m = 1$ only, as previously mentioned). The constants $\mathscr{L}_n$, $\mathscr{Q}_n$, and $\mathscr{N}_1$ were obtained from equations (16), (17), and (18), respectively, the constants $\mathscr{K}_{1,n}$ and $\mathscr{O}_{1,n}$ from equations (14) and (15), respectively, and the constants $\mathscr{M}_{1,n}$ and $\mathscr{P}_{1,n}$ from equations (13). The distribution was found in two planes representing the maximum and minimum temperatures for the Z-axis; the first plane was located at the side of the cross section of the rectangular parallelepiped and the second plane was on the median plane through the rectangular parallelepiped. The results are shown in figure 10(a) for an effective gas temperature of 2000° F and a thermal conductivity of 15 Btu/(hr)(ft)(°F) and give the temperature distribution at various distances from the coolant passage. The curve labeled "approximation of temperature" in figure 10(a) is a one-dimensional chordwise distribution through the approximated rectangular trailing section. Similar results, for thermal conductivities of 120 and 210 Btu/(hr)(ft)(°F) are given in figures 10(b) and 10(c), respectively. Calculation of $\cos \mathscr{N}_1 \tau/2$ (see equation (12)) reveals the temperature variation in the two planes to be about 3.6 percent of θ for a blade thermal conductivity of 15 Btu/(hr)(ft)(°F), 0.5 percent for a thermal conductivity of 120 Btu/(hr)(ft)(°F), and 0.3 percent for a thermal conductivity of 210 Btu/(hr)(ft)(°F). For a thermal conductivity of 15 Btu/(hr)(ft)(°F), figure 10(a) shows a constant temperature for the last three-quarters of the blade; that is, conduction to the rim affects about the first quarter of the blade length. Figure 10(a) also shows that the level of the temperature in the principal portion of the blade rises rapidly as the distance from the coolant passage is increased. Near the coolant passage, the distribution is in good agreement with the one-dimensional spanwise distribution presented in figures 6 and 8. As the thermal conductivity is increased, as shown in figures 10(b) and 10(c), the part of the blade affected by rim conduction increases; for a thermal conductivity of 210 Btu/(hr)(ft)(°F), about two thirds of the blade length shows this effect.

One-Dimensional Chordwise Temperature Distribution through Simplified Shapes

Because the three-dimensional distribution resulted in a constant spanwise blade temperature in the region of the blade beyond the influence of rim cooling and because the critical blade point, as determined from a temperature-stress relation, may likewise be beyond the region of rim-cooling influence, one-dimensional chordwise temperature distributions were obtained. In order to compare the three-dimensional distribution with a one-dimensional chordwise distribution, a rectangular trailing section was first considered. Figure 11 shows this comparison for an effective gas temperature of 2000° F and a blade thermal conductivity of 15 Btu/(hr)(ft)(°F); the one-dimensional distribution was determined by use of equation (19). From figure 11 it can be seen that the trailing-edge temperature increases from 1500° to 1850° F as the distance from the blade root is increased from 0.25 to 1.0 inch for the three-dimensional case, even for low-conductivity material. On the other hand, in the region of the blade beyond the influence of rim cooling (when the distance from the blade root is 1 in. or more), the one-dimensional and three-dimensional results approach identity; for such a region, a three-dimensional solution is unnecessary when low-conductivity materials are considered.

In order to more nearly approximate a blade trailing section, a trapezoidal approximation was considered. For comparative purposes, the trapezoidal and rectangular sections were constructed to have equal lengths and areas. In general, however, the trapezoid is constructed so that the thickness at the coolant passages equals one-half the actual blade surface exposed to the coolant. This dimension, in turn, fixes the length of the trapezoid.

The temperature distribution through a trapezoidal section was obtained by use of equation (20). Such a distribution, for an effective gas temperature of 2000° F and a blade thermal conductivity of 15 Btu/(hr)(ft)(°F), is compared with the distribution through a rectangular section in figure 12. The temperature distribution for the trapezoidal section has a slightly steeper slope than that for the rectangular section at distances remote from the coolant passages and the temperatures at the trailing edge and the coolant-passage wall are lower. Part of this lower temperature for the trapezoidal section is due to the additional thickness of the cooling surface.

The effect of varying thermal conductivity from 15 to 210 Btu/(hr)(ft)(°F) on the temperature distributions along the center line of rectangular and trapezoidal sections is shown in figures 13(a)

and 13(b), respectively. In each case, as thermal conductivity is increased, the temperature distributions flatten and approach linearity, decreasing in the trailing section and increasing near the coolant passages. Figure 14 shows blade trailing-edge temperatures for various thermal conductivities obtained by use of the rectangular and trapezoidal approximations. Cooling is substantially greater for the more representative trapezoidal section. For currently used high-temperature alloys with thermal conductivities in the neighborhood of 15 Btu/(hr)(ft)($^{\circ}$F), figure 14 shows a trailing-edge temperature difference for the rectangular and trapezoidal sections of only about 60° F for an effective gas temperature of 2000° F.

Chordwise temperatures were also calculated, by use of equations (22) to (27), for concentric circle annuli and parallel-plate approximations. These temperatures are not plotted in this report; they were only used as initial approximations for the two-dimensional numerical calculations made for an actual blade shape.

Two-Dimensional Chordwise Temperature Distribution

Two-dimensional temperature distributions were determined for an actual blade shape by application of the relaxation method. Separate calculations were made for the cases where an average gas-to-blade heat-transfer coefficient and where a typical variation in the gas-to-blade heat-transfer coefficient as shown in figure 15 were considered. Initial trial solutions were determined by use of equation (20) for the trailing section, equations (22) to (24) for the leading section, and equations (26) and (27) for the thin-wall sections of the blade near the coolant passages. A comparison of the temperature distributions for assumed variable and constant gas-to-blade heat-transfer coefficients, for an effective gas temperature of 2000° F, an average coolant temperature of 200° F, and a blade thermal conductivity of 15 Btu/(hr)(ft)($^{\circ}$F) is shown in figure 16. The blade temperatures obtained are nearly the same for both cases except at the leading and trailing edges. Use of the average coefficient gives a conservative estimate of the trailing-edge temperature and a temperature that is somewhat too low near the leading edge.

A calculation has also been made for the average gas-to-blade coefficient and for a blade with a thermal conductivity of 100 Btu/(hr)(ft)($^{\circ}$F). A comparison of this solution with the similar one for a thermal conductivity of 15 Btu/(hr)(ft)($^{\circ}$F) is shown in figure 17. The high-conductivity blade has about a 250° and a 600° F lower temperature than the low-conductivity blade at the leading and trailing edges, respectively. Little temperature difference is obtained in the center of the blade, where extremely good cooling prevails.

The results of the various relaxation solutions are in good agreement with the one-dimensional chordwise approximations that were used to start the numerical solutions; that is, good representative temperatures are obtainable by use of one-dimensional chordwise approximations.

In order to determine the effect of distance from the coolant passage on the trailing-edge temperature, trailing-edge temperatures were determined for the liquid-cooled blade with five coolant passages shown in figure 18. Various length trailing sections were obtained by successively reducing the length of the trailing section shown in figure 18. The temperatures were determined by use of equation (20) and are shown for various thermal conductivities in figure 19. The trailing-edge temperature is reduced almost linearly as the length of the trailing section is decreased. The effect of thermal conductivity also decreases as the trailing-section length is decreased.

NONDIMENSIONAL CHARTS

The availability of several nondimensional charts, to be subsequently discussed, eliminates the necessity for some numerical calculation.

The prevalent blade temperature is given by equation (2a) as

$$T_{B,p} = \frac{h_o l_o T_{g,e} + h_{i,2} l_{i,2} T_l}{h_o l_o + h_{i,2} l_{i,2}} \tag{2a}$$

After division by $h_{i,2} l_{i,2}$, this equation may be written

$$T_{B,p} = \frac{T_l + \lambda T_{g,e}}{1+\lambda}$$

where

$$\lambda = \frac{h_o l_o}{h_{i,2} l_{i,2}}$$

Subtraction of $T_{g,e}$ from both members of this equation leads to

$$\frac{T_{g,e} - T_{B,p}}{T_{g,e} - T_l} = \frac{1}{1+\lambda}$$

The plot of $\frac{T_{g,e}-T_{B,p}}{T_{g,e}-T_l}$ against λ is shown in figure 20. For any given blade, λ can be evaluated and the value of $\frac{T_{g,e}-T_{B,p}}{T_{g,e}-T_l}$ can be obtained. Finally, for the desired effective gas and coolant temperatures, a single simple algebraic operation results in the desired value of the prevalent blade temperature.

Another nondimensional chart, which gives the one-dimensional chordwise temperature distribution through a rectangular section, is also presented in figure 21. The temperature distribution through a rectangular section is given by equation (19),

$$T_{g,e}-T_B = \frac{\frac{h_i}{k_B}(T_{g,e}-T_l)\cosh \varphi y'}{\varphi \sinh \varphi j' + \frac{h_i}{k_B}\cosh \varphi j'} \tag{19}$$

For a given turbine and set of turbine operating conditions, values can be determined for all the quantities in this equation. A semilog plot with $\varphi j'$ as abscissa and $h_i/\varphi k_B$ as a parameter results in a nondimensional cooling ratio

$$\frac{T_{g,e}-T_B}{(T_{g,e}-T_l)\cosh \varphi y'}$$

The addition of a second quadrant, with $\cosh \varphi y'$ as parameter, yields values of the temperature ratio $\frac{T_{g,e}-T_B}{T_{g,e}-T_l}$ at any point in the rectangular section. This chart is given in figure 21. The chart is used as follows: A vertical line is constructed through the calculated value of the abscissa $\varphi j'$ and is extended to the calculated value of the parameter $h_i/\varphi k_B$. From this point, a horizontal line is drawn, extending into the second quadrant, and intersecting several lines representing various values of $\cosh \varphi y'$. Vertical lines from the intersection points to the abscissa in the second quadrant give values of the temperature ratio $\frac{T_{g,e}-T_B}{T_{g,e}-T_l}$ at various positions in the rectangular section. Values of the temperature T_B are then easily obtainable.

In order to illustrate the use of figure 21, a rectangular section with dimensions equal to those previously tabulated will be considered. For a blade thermal conductivity of 15 Btu/(hr)(ft)(^{o}F) and outside and inside heat-transfer coefficients of 222 and 2370 Btu/(hr)(sq ft)(^{o}F), respectively, the parameters used in figure 21 are evaluated as follows:

$$\varphi j = \left(\frac{2h_o}{k_B \tau}\right)^{\frac{1}{2}} j = \left[\frac{2(222)}{15(0.01)}\right]^{\frac{1}{2}} (0.055) = 3$$

$$\frac{h_i}{\varphi k_B} = \frac{2370}{(54.4)(15)} = 2.9$$

The point represented by these parameters is given by the symbol ○ in the first quadrant of figure 21; the symbol □ on figure 21 designates the corresponding point for a thermal conductivity of 210 Btu/(hr)(ft)(^{o}F). A horizontal line passing through the symbol ○ and intersecting the family of lines in the second quadrant of figure 21 gives as the abscissa of the second quadrant the values of the temperature ratio $\frac{T_{g,e}-T_B}{T_{g,e}-T_l}$ for various positions in the rectangular section as follows:

$$\frac{T_{g,e}-T_B}{T_{g,e}-T_l} = 0.075 \quad \text{for} \quad \varphi y' = 0$$

$$= 0.115 \quad \text{for} \quad \varphi y' = 1$$

$$= 0.285 \quad \text{for} \quad \varphi y' = 2$$

$$= 0.75 \quad \text{for} \quad \varphi y' = 3$$

For $T_{g,e} = 2000^{o}$ F and $T_l = 200^{o}$ F, it follows that the blade-temperature calculation results in the following values:

$T_B = 1865$ for $\varphi y' = 0$ (trailing-edge temperature)

$= 1793$ for $\varphi y' = 1$

$= 1487$ for $\varphi y' = 2$

$= 650$ for $\varphi y' = 3$ (temperature at coolant passage)

These results compare favorably with the calculated distribution shown on figure 12.

CONCLUDING REMARKS

Analyses have been presented for obtaining spanwise temperature distributions near a coolant passage, chordwise distributions (for both approximated and actual shapes) in regions where conduction to the rim is inappreciable, and three-dimensional distributions for approximated blade shapes. Numerical examples based on specific blade configurations and heat-transfer coefficients available from unclassified sources have been presented. Although the analyses are exact, the numerical values used in the calculations may not necessarily be the same as those for cooled turbines. The numerical examples have been presented to indicate the range of applicability of the various analyses and to present the general nature of temperature distributions in liquid-cooled turbine blades. In the following paragraphs the more important results are reviewed to show their general guidance for design studies.

The three-dimensional temperature distribution includes conduction to the rim, whereas the two-dimensional and one-dimensional chordwise distributions do not. Consequently, the temperatures obtained from a three-dimensional investigation are less than those otherwise obtained. As a result, it is advisable to determine the simplified solutions first; if the temperatures that result are not excessively high, a three-dimensional investigation is unnecessary; whereas if the resulting temperatures are large, a three-dimensional investigation can be made.

The two-dimensional solution just referred to is of necessity a numerical solution (because of the varying boundary condition caused by the shape of the blade). It has been shown by the calculations previously presented that for uniform outside heat-transfer coefficients, simplified one-dimensional distributions were in excellent agreement with the two-dimensional relaxation solution. When variable outside heat-transfer coefficients were considered, the simplified solutions indicated optimistic results and the two-dimensional relaxation solution appears essential. Increasing blade thermal conductivity results in raising the cooling surface temperature and lowering the trailing-edge temperature and thus is a more uniform blade temperature.

One-dimensional spanwise distributions proved to be valid near the coolant passages. The temperature of the cooled part of the blade (prevalent blade temperature) was independent of blade length. If the inside heat-transfer coefficient is increased, the prevalent blade temperature decreases; it was shown for a particular case that the prevalent blade temperature for water as coolant was only about half that for kerosene as coolant.

Lewis Flight Propulsion Laboratory,
National Advisory Committee for Aeronautics,
Cleveland, Ohio, October 27, 1950.

APPENDIX A

SYMBOLS

The following symbols are used in this report:

A	area of metal, sq ft
b	blade span, ft
$C_1, \ldots, C_{11}$	constants of integration
D	diameter of circle used to approximate leading section of blade, ft
d	ratio of distance between net points 0 and 5 and net spacing
H_1 iH_o	Hankel functions (special kinds of Bessel function)
h	heat-transfer coefficient, Btu/(sec)(sq ft)($^\circ$F) or Btu/(hr)(sq ft)($^\circ$F)
J_o iJ_1	Bessel functions
j	chordwise distance from blade trailing edge to coolant passage, ft
K	$\left(\frac{h_o}{k_B \sin \psi}\right)^{\frac{1}{2}}$
k	thermal conductivity, Btu/(sec)(ft)($^\circ$F) or Btu/(hr)(ft)($^\circ$F)
l	perimeter, ft
M,N,O,P	points on figure 3
Q	heat flow, Btu/sec

r radial distance from hub of turbine, ft

T temperature, ^{o}F

x distance from blade tip to blade element, ft

y distance from trailing edge to blade element, ft

Z number of blades

z distance from median plane of section to blade element, ft

Γ $H_1(i\zeta_1)J_o(i\zeta_2) + iJ_1(i\zeta_1)iH_o(i\zeta_2)$

ζ $2K\left[y' + \frac{\tau_1(1-\tan\psi)}{2\tan\psi}\right]^{\frac{1}{2}}$

θ $T_{g,e}-T_B$

λ $\frac{h_o l_o}{h_{i,2} l_{i,2}}$

σ distance between parallel plates, ft

τ thickness of trailing section, ft

φ $\left(\frac{2h_o}{k_B \tau}\right)^{\frac{1}{2}}$

ψ $\tan^{-1}\left(\frac{\tau_2-\tau_1}{2j}\right)$

Subscripts:

a air

av average

B blade

e effective

g gas

i inside (inner with D)

l liquid

m, n } summation indices

o outside (outer with D)

p prevalent

R rotor

r blade root

rim rim

T blade tip

1, 2, 3, 4 } denote sections in spanwise investigation when used with x; 1 and 2 denote trapezoidal thicknesses at trailing edge and coolant passage, respectively, when used with τ

α, β } denote end near blade tip and end near rotor hub of various sections

Superscript:

prime linear dimension increased by $\tau/2$

Functions:

$\mathscr{A}$ $\left(\frac{h_o l_o}{k_B A_{B,l}}\right)^{\frac{1}{2}}$

$\mathscr{B}$ $\left(\frac{h_o l_o + h_{i,2} l_{i,2}}{k_B A_{B,2}}\right)^{\frac{1}{2}}$

$\mathscr{D}$ $\left(\frac{h_o l_o T_{g,e} + h_{i,2} l_{i,2} T_l}{k_B A_{B,2}}\right)^{\frac{1}{2}}$

$\mathscr{E}$ $\left[\frac{4\pi r_{3,av} h_a + (h_{i,3} l_{i,3})_{av}}{k_{rim} A_{rim}}\right]^{\frac{1}{2}}$

$\mathscr{F}$ $\left[\frac{4\pi r_{3,av} h_a T_a + (h_{i,3} l_{i,3})_{av} T_l}{k_{rim} A_{rim}}\right]^{\frac{1}{2}}$

$\mathscr{G}$ $\left(\frac{\mathscr{F}}{\mathscr{E}}\right)^2$

$\mathscr{H}$ $\left[\frac{4\pi r_{4,av} h_a + (h_{i,4} l_{i,4})_{av}}{k_R A_R}\right]^{\frac{1}{2}}$

$\mathscr{I}$ $\left[\frac{4\pi r_{4,av} h_a T_a + (h_{i,4} l_{i,4})_{av} T_l}{k_R A_R}\right]^{\frac{1}{2}}$

$\mathscr{J}$ $\left(\frac{\mathscr{I}}{\mathscr{H}}\right)^2$

$\mathscr{K}, \mathscr{L}, \mathscr{M}, \mathscr{N}, \mathscr{O}, \mathscr{P}, \mathscr{Q}$ integration constants (See equations (13) to (18).)

$\mathscr{R}$ $k_B \mathscr{M}_{m,n} \sinh \mathscr{M}_{m,n} j' + h_i \cosh \mathscr{M}_{m,n} j'$

$$\mathscr{S}_n \quad \frac{4h_i}{\pi} (T_{g,e} - T_l) \frac{(-1)^{n-1}}{2n-1}$$

$$\mathscr{T}_n \quad 2(T_{g,e} - T_{B,r}) \left(\frac{\sin \mathscr{Q}_{nj'}}{\mathscr{Q}_{nj'}} \right) \left(\frac{1}{1 + \frac{\sin 2\mathscr{Q}_{nj'}}{2\mathscr{Q}_{nj'}}} \right)$$

APPENDIX B

ONE-DIMENSIONAL SPANWISE TEMPERATURE DISTRIBUTION

The heat balance for the uncooled section of the blade (fig. 1, section 1) is given as follows:

$$\text{Heat entering by radial conduction} = - k_B A_{B,1} \frac{dT_{B,1}}{dx_1}$$

$$\text{Heat entering sides by convection} = h_o l_o (T_{g,e} - T_{B,1})\, dx_1$$

$$\text{Heat leaving by radial conduction} = - k_B A_{B,1} \frac{d}{dx_1}\left(T_{B,1} + \frac{dT_{B,1}}{dx_1} dx_1\right)$$

The heat-balance equation is

$$- k_B A_{B,1} \frac{dT_{B,1}}{dx_1} + h_o l_o (T_{g,e} - T_{B,1})\, dx_1 = - k_B A_{B,1} \frac{d}{dx_1}\left(T_{B,1} + \frac{dT_{B,1}}{dx_1} dx_1\right)$$

or

$$\frac{d^2 T_{B,1}}{dx_1^2} - \mathscr{A}^2 T_{B,1} = - \mathscr{A}^2 T_{g,e} \tag{B1}$$

where

$$\mathscr{A} = \left(\frac{h_o l_o}{k_B A_{B,1}}\right)^{\frac{1}{2}}$$

A solution is

$$T_{B,1} = T_{g,e} - C_1 \cosh \mathscr{A}(x_1 + C_2) \tag{1}$$

where C_1 and C_2 are integration constants.

For the cooled section of the blade (fig. 1, section 2) the heat balance is given as follows:

Heat entering by radial conduction = $- k_B A_{B,2} \frac{dT_{B,2}}{dx_2}$

Heat entering sides by convection = $h_o l_o (T_{g,e} - T_{B,2}) \, dx_2$

Heat leaving by radial conduction = $- k_B A_{B,2} \frac{d}{dx_2} \left(T_{B,2} + \frac{dT_{B,2}}{dx_2} \, dx_2 \right)$

Heat leaving by radial convection = $h_{i,2} l_{i,2} (T_{B,2} - T_l) \, dx_2$

The heat-balance equation is

$$- k_B A_{B,2} \frac{dT_{B,2}}{dx_2} + h_o l_o (T_{g,e} - T_{B,2}) \, dx_2 =$$

$$- k_B A_{B,2} \frac{d}{dx_2} \left(T_{B,2} + \frac{dT_{B,2}}{dx_2} \, dx_2 \right) + h_{i,2} l_{i,2} (T_{B,2} - T_l) \, dx_2$$

or

$$\frac{d^2 T_{B,2}}{dx_2^2} - \mathscr{B}^2 T_{B,2} = - \mathscr{D}^2 \tag{B2}$$

where

$$\mathscr{B} = \left(\frac{h_o l_o + h_{i,2} l_{i,2}}{k_B A_{B,2}} \right)^{\frac{1}{2}}$$

and

$$\mathscr{D} = \left(\frac{h_o l_o T_{g,e} + h_{i,2} l_{i,2} T_l}{k_B A_{B,2}} \right)^{\frac{1}{2}}$$

A solution is

$$T_{B,2} = T_{B,p} - C_3 e^{\mathscr{B}x_2} - C_4 e^{-\mathscr{B}x_2} \tag{2}$$

where C_3 and C_4 are integration constants and

$$T_{B,p} = \left(\frac{\mathscr{D}}{\mathscr{B}}\right)^2 = \frac{h_o l_o T_{g,e} + h_{i,2} l_{i,2} T_l}{h_o l_o + h_{i,2} l_{i,2}}$$

For the rim section (assumed constant area) of the rotor (fig. 1, section 3), curvature was neglected because the rim thickness was small in comparison with the rim radius. In addition, average values of $h_{i,3} l_{i,3}$ and r_3 were used. The heat-balance equation reduced to

$$\frac{d^2 T_{rim}}{dx_3^2} - \mathscr{E}^2 T_{rim} = -\mathscr{F}^2 \tag{B3}$$

where

$$\mathscr{E}^2 = \frac{4\pi r_{3,av} h_a + (h_{i,3} l_{i,3})_{av}}{k_{rim} A_{rim}}$$

and

$$\mathscr{F}^2 = \frac{4\pi r_{3,av} h_a T_a + (h_{i,3} l_{i,3})_{av} T_l}{k_{rim} A_{rim}}$$

A solution is

$$T_{rim} = \mathscr{G} + C_5 e^{\mathscr{E}x_3} + C_6 e^{-\mathscr{E}x_3} \tag{3}$$

where C_5 and C_6 are integration constants and where

$$\mathscr{G} = \left(\frac{\mathscr{F}}{\mathscr{E}}\right)^2$$

For the rotor section (assumed constant strength) (fig. 1, section 4), average values are used for $h_{i,4}l_{i,4}$ and for r_4, and an approximate solution (as in section 3) is obtained. Because the rotor is liquid-cooled, such a solution is adequate. The resulting differential equation for this section is

$$\frac{d^2T_R}{dr^2} - \mathscr{H}^2 T_R = - \mathscr{I}^2 \tag{B4}$$

where

$$\mathscr{H}^2 = \frac{4\pi r_{4,av}h_a + (h_{i,4}l_{i,4})_{av}}{k_R A_R}$$

and

$$\mathscr{I}^2 = \frac{4\pi r_{4,av}h_a T_a + (h_{i,4}l_{i,4})_{av}T_l}{k_R A_R}$$

A solution is

$$T_R = \mathscr{J} + C_7 \cosh \mathscr{H}r \tag{4}$$

where C_7 is an integration constant and where

$$\mathscr{J} = \left(\frac{\mathscr{I}}{\mathscr{H}}\right)^2$$

The boundary condition

$$\frac{dT_R}{dr} = 0 \quad \text{for} \quad r = 0$$

has already been applied.

APPENDIX C

THREE-DIMENSIONAL TEMPERATURE DISTRIBUTION THROUGH SIMPLIFIED TRAILING SECTION

A three-dimensional temperature distribution through a rectangular parallelepiped, an approximation for the trailing section of a liquid-cooled turbine blade, is given as follows (fig. 2):

$$\text{Heat entering element from top} = - k_B \, dy \, dz \, \frac{\partial T_B}{\partial x}$$

$$\text{Heat entering element from right end} = - k_B \, dx \, dz \, \frac{\partial T_B}{\partial y}$$

$$\text{Heat entering element from front} = - k_B \, dx \, dy \, \frac{\partial T_B}{\partial z}$$

$$\text{Heat leaving element at bottom} = - k_B \, dy \, dz \left(\frac{\partial T_B}{\partial x} + \frac{\partial^2 T_B}{\partial x^2} \, dx \right)$$

$$\text{Heat leaving element at left end} = - k_B \, dx \, dz \left(\frac{\partial T_B}{\partial y} + \frac{\partial^2 T_B}{\partial y^2} \, dy \right)$$

$$\text{Heat leaving element at rear} = - k_B \, dx \, dy \left(\frac{\partial T_B}{\partial z} + \frac{\partial^2 T_B}{\partial z^2} \, \partial z \right)$$

The heat-balance equation is

$$- k_B \, dy \, dz \, \frac{\partial T_B}{\partial x} - k_B \, dx \, dz \, \frac{\partial T_B}{\partial y} - k_B \, dx \, dy \, \frac{\partial T_B}{\partial z} =$$

$$- k_B \, dy \, dz \left(\frac{\partial T_B}{\partial x} + \frac{\partial^2 T_B}{\partial x^2} \, dx \right) - k_B \, dx \, dz \left(\frac{\partial T_B}{\partial y} + \frac{\partial^2 T_B}{\partial y^2} \, dy \right) -$$

$$k_B \, dx \, dy \left(\frac{\partial T_B}{\partial z} + \frac{\partial^2 T_B}{\partial z^2} \, \partial z \right)$$

or

$$\frac{\partial^2 T_B}{\partial x^2} + \frac{\partial^2 T_B}{\partial y^2} + \frac{\partial^2 T_B}{\partial z^2} = 0 \tag{C1}$$

Simplification in applying boundary conditions results from the use of the effective gas temperature $T_{g,e}$ instead of the blade temperature T_B as the reference temperature, that is, by use of the substitution

$$\theta = T_{g,e} - T_B$$

Equation (C1) then becomes

$$\frac{\partial^2 \theta}{\partial x'^2} + \frac{\partial^2 \theta}{\partial y'^2} + \frac{\partial^2 \theta}{\partial z^2} = 0 \tag{11}$$

The origin of the coordinates chosen is shown in figure 2; the plane $z = 0$ is the median plane of the rectangular parallelepiped and from considerations of symmetry no heat flows across this median plane. The boundary conditions to be applied are

$$\frac{\partial \theta}{\partial x'} = 0 \quad \text{when} \quad x' = 0 \tag{C2}$$

$$\frac{\partial \theta}{\partial y'} = 0 \quad \text{when} \quad y' = 0 \tag{C3}$$

$$\frac{\partial \theta}{\partial z} = 0 \quad \text{when} \quad z = 0 \tag{C4}$$

$$\theta = T_{g,e} - T_{B,r} \quad \text{when} \quad x' = b' \tag{C5}$$

$$k_B \frac{\partial \theta}{\partial y} = h_i (T_{g,e} - T_l - \theta) \quad \text{when} \quad y' = j' \tag{C6}$$

and

$$k_B \frac{\partial \theta}{\partial z} = - h_o \theta \quad \text{when} \quad z = \tau/2 \tag{C7}$$

A solution of equation (11) satisfying the three boundary conditions (C2), (C3), and (C4) is

$$\theta = \sum_{m=1}^{\infty}\sum_{n=1}^{\infty} (\mathscr{K}_{m,n} \cos \mathscr{L}_n x' \cosh \mathscr{M}_{m,n} y' \cos \mathscr{N}_m z + \mathscr{O}_{m,n} \cosh \mathscr{P}_{m,n} x' \cos \mathscr{Q}_n y' \cos \mathscr{N}_m z) \tag{12}$$

where $\mathscr{K}$, $\mathscr{L}$, $\mathscr{M}$, $\mathscr{N}$, $\mathscr{O}$, $\mathscr{P}$, and $\mathscr{Q}$ are constants. Relations among these constants are

$$\left.\begin{aligned} \mathscr{M}_{m,n}^2 &= \mathscr{N}_m^2 + \mathscr{L}_n^2 \\ \mathscr{P}_{m,n}^2 &= \mathscr{N}_m^2 + \mathscr{Q}_n^2 \end{aligned}\right\} (m,n = 1,2,3, \ldots) \tag{13}$$

The boundary condition expressed by equation (C5) leads to a determination of $\mathscr{L}$. Substitution of equation (12) into equation (C5) gives

$$T_{g,e} - T_{B,r} = \sum_{m=1}^{\infty}\sum_{n=1}^{\infty} (\mathscr{K}_{m,n} \cos \mathscr{L}_n b' \cosh \mathscr{M}_{m,n} y' \cos \mathscr{N}_m z + \mathscr{O}_{m,n} \cosh \mathscr{P}_{m,n} b' \cos \mathscr{Q}_n y' \cos \mathscr{N}_m z) \tag{C8}$$

It can be seen that the first member in the double summation in equation (12) vanishes when $\cos \mathscr{L}_n x' = 0$; hence, if

$$\mathscr{L}_n = \left(n - \frac{1}{2}\right)\frac{\pi}{b'}$$

from equation (C8) it follows that

$$T_{g,e} - T_{B,r} = \sum_{m=1}^{\infty}\sum_{n=1}^{\infty} \mathscr{O}_{m,n} \cosh \mathscr{P}_{m,n} b' \cos \mathscr{Q}_n y' \cos \mathscr{N}_m z \tag{C9}$$

This is a Fourier development along y' and z.

The development of equation (C6) leads to a determination of $\mathcal{Q}_n$. Equation (C6) becomes, with the aid of equation (12) and its derivative

$$\sum_{m=1}^{\infty}\sum_{n=1}^{\infty} k_B \left[\mathcal{K}_{m,n} (\cos \mathcal{L}_n x') \mathcal{M}_{m,n} \sinh \mathcal{M}_{m,n} j' \cos \mathcal{N}_m z - \mathcal{O}_{m,n} (\cosh \mathcal{P}_{m,n} x') \mathcal{Q}_n \sin \mathcal{Q}_n j' \cos \mathcal{N}_m z\right]$$

$$= \sum_{m=1}^{\infty}\sum_{n=1}^{\infty} h_i \left(T_{g,e} - T_l - \mathcal{K}_{m,n} \cos \mathcal{L}_n x' \cosh \mathcal{M}_{m,n} j' \cos \mathcal{N}_m z - \mathcal{O}_{m,n} \cosh \mathcal{P}_{m,n} x' \cos \mathcal{Q}_n j' \cos \mathcal{N}_m z\right) \quad (C10)$$

In order to simplify equation (C10) at the boundary when $y' = j'$ and to solve for the constant $\mathcal{Q}_n$, the second summation in the left member is equated to the last summation in the right member term by term. Then

$$h_i(T_{g,e} - T_l) = \sum_{m=1}^{\infty}\sum_{n=1}^{\infty} \mathcal{K}_{m,n} (k_B \mathcal{M}_{m,n} \sinh \mathcal{M}_{m,n} j' + h_i \cosh \mathcal{M}_{m,n} j') \cos \mathcal{L}_n x' \cos \mathcal{N}_m z \quad (C11)$$

and

$$\sum_{m=1}^{\infty}\sum_{n=1}^{\infty} k_B \mathcal{O}_{m,n} (\cosh \mathcal{P}_{m,n} x') \mathcal{Q}_n \sin \mathcal{Q}_n j' \cos \mathcal{N}_m z$$

$$= \sum_{}^{\infty}\sum_{}^{\infty} h_i \mathcal{O}_{m,n} \cosh \mathcal{P}_{m,n} x' \cos \mathcal{Q}_n j' \cos \mathcal{N}_m z \quad (C12)$$

The sums are equated term by term. Therefore, $\mathcal{Q}_n$ is determined as any solution of

$$\tan\left(\mathcal{Q}_n j'\right) = \frac{h_i}{k_B \mathcal{Q}_n} = \frac{\frac{h_i j'}{k_B}}{\mathcal{Q}_n j'} \tag{17}$$

The development of equation (C7) leads to a determination of $\mathcal{N}_m$.

$$\sum_{m=1}^{\infty}\sum_{n=1}^{\infty} - k_B\left[\mathcal{K}_{m,n} \cos \mathcal{L}_n x' \cosh \mathcal{M}_{m,n} y' \left(\mathcal{N}_m \sin \mathcal{N}_m \frac{\tau}{2}\right) + \mathcal{O}_{m,n} \cosh \mathcal{P}_{m,n} x' \cos \mathcal{Q}_n y' \left(\mathcal{N}_m \sin \mathcal{N}_m \frac{\tau}{2}\right)\right]$$

$$= \sum_{m=1}^{\infty}\sum_{n=1}^{\infty} - h_o\left(\mathcal{K}_{m,n} \cos \mathcal{L}_n x' \cosh \mathcal{M}_{m,n} y' \cos \mathcal{N}_m \frac{\tau}{2} + \mathcal{O}_{m,n} \cosh \mathcal{P}_{m,n} x' \cos \mathcal{Q}_n y' \cos \mathcal{N}_m \frac{\tau}{2}\right) \tag{C13}$$

or

$$\tan \mathcal{N}_m \frac{\tau}{2} = \frac{h_o}{k_B \mathcal{N}_m} = \frac{\frac{h_o \tau}{2k_B}}{\frac{\mathcal{N}_m \tau}{2}} \tag{18}$$

The possibility of determining values of $\mathcal{K}_{m,n}$ and $\mathcal{O}_{m,n}$ to satisfy equations (C9) and (C11) has been established in textbooks on Fourier and other harmonic series (reference 7, pp. 118-121), and it is only necessary that the values determined define a convergent series.

Values of $\mathcal{K}_{m,n}$ are determined by integrating equation (C11) between the limits $x' = 0$ to $x' = b'$ and $z = 0$ to $z = \tau/2$ and substituting the values previously determined for $\mathcal{L}_n$ and $\mathcal{N}_m$ in equations (16) and (18). The integration is accomplished in two steps

using the functions $\cos \mathscr{L}_s x' \, dx'$ and $\cos \mathscr{N}_v z \, dz$ as multipliers, where s and v are integers. For abbreviation,

$$\mathscr{R} = k_B \mathscr{M}_{m,n} \sinh \mathscr{M}_{m,n} j' + h_i \cosh \mathscr{M}_{m,n} j' \tag{C14}$$

Then

$$\sum_{m=1}^{\infty} \mathscr{R}\mathscr{K}_{m,n} \cos \mathscr{N}_m z \int_{x'=0}^{x'=b'} \cos^2 \mathscr{L}_n x' \, dx'$$

$$= h_i (T_{g,e} - T_l) \int_{x'=0}^{x'=b'} \cos \mathscr{L}_n x' \, dx' \tag{C15}$$

because all the terms

$$\int_0^{b'} \cos \mathscr{L}_n x' \cos \mathscr{L}_s x' \, dx'$$

vanish if $s \neq n$. Integration of equation (C15) and substitution of limits leads to the result

$$\sum_{m=1}^{\infty} \mathscr{R}\mathscr{K}_{m,n} \frac{\cos \mathscr{N}_m z}{2\mathscr{L}_n} \left[\mathscr{L}_n x' + \frac{\sin 2 \mathscr{L}_n x'}{2} \right]_0^{b'}$$

$$= h_i \left[\frac{(T_{g,e} - T_l)}{\mathscr{L}_n} \sin \mathscr{L}_n x' \right]_0^{b'} \tag{C16}$$

or

$$\sum_{m=1}^{\infty} \mathscr{R}\mathscr{K}_{m,n} \cos \mathscr{N}_m z \left(b' + \frac{\sin 2 \mathscr{L}_n b'}{2\mathscr{L}_n} \right)$$

$$= 2h_i (T_{g,e} - T_l) \frac{\sin \mathscr{L}_n b'}{\mathscr{L}_n} \tag{C17}$$

When equation (16) is used for $\mathcal{S}_n$, there results

$$\sum_{m=1}^{\infty} \mathcal{R}\mathcal{K}_{m,n} \cos \mathcal{N}_m z = \frac{4}{\pi} h_i (T_{g,e} - T_l) \frac{(-1)^{n-1}}{(2n-1)} = \mathcal{S}_n \tag{C18}$$

When equation (C18) is integrated in terms of z, using the multiplier $\cos \mathcal{M}_v z \, dz$, it follows that

$$\mathcal{R}\mathcal{K}_{m,n} \int_{z=0}^{z=\frac{\tau}{2}} \cos^2 \mathcal{N}_m z \, dz = \mathcal{S}_n \int_{z=0}^{z=\frac{\tau}{2}} \cos \mathcal{N}_m z \, dz \tag{C19}$$

because all the terms

$$\int_0^{\frac{\tau}{2}} \cos \mathcal{N}_m z \cos \mathcal{N}_v z \, dz$$

vanish if $m \neq v$. Upon integration,

$$\frac{\mathcal{R}\mathcal{K}_{m,n}}{2\mathcal{N}_m} \left(\mathcal{N}_m z + \frac{\sin 2\mathcal{N}_m z}{2} \right)_0^{\frac{\tau}{2}} = \frac{\mathcal{S}_n}{\mathcal{N}_m} \left(\sin \mathcal{N}_m z \right)_0^{\frac{\tau}{2}} \tag{C20}$$

or

$$\mathcal{R}\mathcal{K}_{m,n} \left(\frac{\tau}{2} + \frac{\sin 2\mathcal{N}_m \frac{\tau}{2}}{2\mathcal{N}_m} \right) = \frac{2\mathcal{S}_n \sin \mathcal{N}_m \frac{\tau}{2}}{\mathcal{N}_m} \tag{C21}$$

Therefore,

$$\mathcal{K}_{m,n} = \frac{2\mathcal{S}_n}{\mathcal{N}_m \frac{\tau}{2}} \frac{\sin \mathcal{N}_m \frac{\tau}{2}}{\left(1 + \frac{\sin 2\mathcal{N}_m \frac{\tau}{2}}{2\mathcal{N}_m \frac{\tau}{2}} \right)} \frac{1}{\mathcal{R}} \tag{C22}$$

Similarly, from equation (C9) it is found that

$$\mathscr{O}_{m,n} = 2\mathscr{T}_n \frac{\sin \mathscr{N}_m \frac{\tau}{2}}{\mathscr{N}_m \frac{\tau}{2}} \frac{1}{\cosh \mathscr{P}_{m,n} b' \left(1 + \frac{\sin 2\mathscr{N}_m \frac{\tau}{2}}{2\mathscr{N}_m \frac{\tau}{2}}\right)} \tag{C23}$$

where

$$\mathscr{T}_n = 2(T_{g,e} - T_{B,r}) \frac{\sin \mathscr{Q}_n j'}{\mathscr{Q}_n j'} \frac{1}{\left(1 + \frac{\sin 2\mathscr{Q}_n j'}{2\mathscr{Q}_n j'}\right)} \tag{C24}$$

Finally, substitution of equations (C14) and (C18) in equation (C22) and substitution of equation (C24) in equation (C23) lead to the following values of the coefficients $\mathscr{K}_{m,n}$ and $\mathscr{O}_{m,n}$:

$$\mathscr{K}_{m,n} = \frac{(-1)^{n-1}}{\pi(2n-1)} \frac{\sin \mathscr{N}_m \frac{\tau}{2}}{\mathscr{N}_m \frac{\tau}{2}} \frac{8h_i(T_{g,e} - T_l)}{\left(1 + \frac{\sin 2\mathscr{N}_m \frac{\tau}{2}}{2\mathscr{N}_m \frac{\tau}{2}}\right)}$$

$$\left(\frac{1}{k_B \mathscr{M}_{m,n} \sinh \mathscr{M}_{m,n} j' + h_i \cosh \mathscr{M}_{m,n} j'}\right) \tag{14}$$

and

$$\mathscr{O}_{m,n} = \frac{\sin \mathscr{Q}_n j'}{\mathscr{Q}_n j'} \frac{4(T_{g,e} - T_{B,r})}{\left(1 + \frac{\sin 2\mathscr{Q}_n j'}{2\mathscr{Q}_n j'}\right)} \frac{\sin \mathscr{N}_m \frac{\tau}{2}}{\mathscr{N}_m \frac{\tau}{2}}$$

$$\frac{1}{\left(1 + \frac{\sin 2\mathscr{N}_m \frac{\tau}{2}}{2\mathscr{N}_m \frac{\tau}{2}}\right)} \frac{1}{\cosh \mathscr{P}_{m,n} b'} \tag{15}$$

APPENDIX D

ONE-DIMENSIONAL CHORDWISE TEMPERATURE DISTRIBUTION THROUGH SIMPLIFIED SHAPES

Rectangular trailing section of blade removed from influence of rim cooling. - The heat balance for an element of the rectangular section is given as follows (fig. 4(a)):

Heat entering by conduction (right end) = $k_B \tau \frac{d\theta}{dy}$

Heat entering by convection (sides) = $2h_o\theta\ dy$

Heat leaving by conduction (left end) = $k_B \tau \left(\frac{d\theta}{dy} + \frac{d^2\theta}{dy^2}\ dy\right)$

The heat-balance equation is

$$k_B \tau \frac{d\theta}{dy} + 2h_o\theta\ dy = k_B \tau \left(\frac{d\theta}{dy} + \frac{d^2\theta}{dy^2}\ dy\right)$$

or

$$\frac{d^2\theta}{dy^2} = \varphi^2\theta \tag{D1}$$

where

$$\varphi = \left(\frac{2h_o}{k_B \tau}\right)^{\frac{1}{2}}$$

A solution is

$$\theta = C_8 \cosh \varphi(y + C_9) \tag{D2}$$

where C_8 and C_9 are integration constants. The boundary conditions to be applied in the evaluation of the integration constants are

$$k_B\tau \frac{d\theta}{dy} = h_i\tau(T_B-T_l) = h_i\tau(T_{g,e}-T_l-\theta) \quad \text{when} \quad y = j \tag{D3}$$

and

$$k_B \frac{d\theta}{dy} = h_o\theta \quad \text{when} \quad y = 0 \tag{D4}$$

From equations (D2) and (D4), it follows that

$$k_B C_8 \varphi \sinh(\varphi C_9) = h_o C_8 \cosh(\varphi C_9)$$

and therefore

$$C_9 = \frac{\tanh^{-1}\left(\frac{h_o}{k_B\varphi}\right)}{\varphi} = \frac{\tanh^{-1}\left(\frac{\varphi\tau}{2}\right)}{\varphi} \approx \frac{\tau}{2} \tag{D5}$$

when τ is not too large. Calculations revealed that the difference between C_9 and $\tau/2$ varied from 0.4 to 0.5 percent for the values of φ considered and had no appreciable effect 0.005 foot or more inside the trailing edge.

From equations (D2), (D3), and (D5) it follows that

$$k_B\tau C_8 \varphi \sinh(\varphi j') = h_i\tau\left[T_{g,e}-T_l-C_8 \cosh(\varphi j')\right]$$

and therefore

$$C_8 = \frac{\frac{h_i}{k_B}(T_{g,e}-T_l)}{\varphi \sinh(\varphi j') + \frac{h_i}{k_B}\cosh(\varphi j')} \tag{D6}$$

Substitution of equations (D5) and (D6) in equation (D2) leads to the final equation

$$\theta = \frac{\frac{h_i}{k_B}(T_{g,e}-T_l)\cosh(\varphi y')}{\varphi \sinh(\varphi j') + \frac{h_i}{k_B}\cosh(\varphi j')} \tag{19}$$

Trapezoidal trailing section of a blade removed from influence of rim cooling. - In reference 8, the temperature-distribution equation along the axis of a trapezoidal section is derived. The solution obtained is expressed by the relation

$$\theta = C_{10}J_o(i\zeta) + C_{11}iH_o(i\zeta) \tag{D7}$$

where C_{10} and C_{11} are integration constants, J_o and iH_o are Bessel functions, and ζ is defined as

$$\zeta^2 = 4K^2\left[y' + \frac{\tau_1(1 - \tan\psi)}{2\tan\psi}\right] \tag{D8}$$

where

$$K^2 = \frac{h_o}{k_B \sin\psi} \tag{D9}$$

and

$$\psi = \tan^{-1}\left(\frac{\tau_2 - \tau_1}{2j}\right) \tag{D10}$$

The constants C_{10} and C_{11} in equation (D7) may be evaluated by application of the following boundary conditions:

$$\frac{d\theta}{dy'} = 0 \quad \text{when} \quad y' = 0 \tag{D11}$$

and

$$k_B \frac{d\theta}{dy'} = h_i(T_{g,e} - T_l - \theta) \quad \text{when} \quad y' = j' \tag{D12}$$

or

$$\frac{d\theta}{d\zeta} = 0 \quad \text{when} \quad \zeta = \zeta_1 \tag{D13}$$

and

$$\frac{k_B 2K^2}{\zeta_2 \frac{d\theta}{d\zeta}} = h_i(T_{g,e}-T_l-\theta) \quad \text{when} \quad \zeta = \zeta_2 \tag{D14}$$

It follows from equation (D8) that when $y' = 0$,

$$\zeta_1 = 2K\left[\frac{\tau_1(1 - \tan\psi)}{2 \tan\psi}\right]^{\frac{1}{2}} \tag{D15}$$

and when $y' = j'$,

$$\zeta_2 = 2K\left[j' + \frac{\tau_1(1 - \tan\psi)}{2 \tan\psi}\right]^{\frac{1}{2}} \tag{D16}$$

Differentiation of equation (D8) gives

$$\frac{d\theta}{d\zeta} = \frac{\zeta}{2K^2}\frac{d\theta}{dy'} \tag{D17}$$

hence,

$$\frac{d\theta}{d\zeta} = 0 \quad \text{when} \quad \frac{d\theta}{dy'} = 0$$

From the properties of the Bessel functions,

$$\frac{dJ_o(y)}{dy} = - J_1(y)$$

and

$$\frac{dH_o(y)}{dy} = - H_1(y)$$

Differentiation of equation (D7) therefore gives

$$\frac{d\theta}{d\zeta} = - C_{10} i J_1(i\zeta) + C_{11} H_1(i\zeta) \tag{D18}$$

and it follows that

$$C_{11} = \frac{C_{10} i J_1(i\zeta_1)}{H_1(i\zeta_1)} \tag{D19}$$

when

$$\frac{d\theta}{d\zeta} = 0$$

From equation (D12), with the use of equations (D7) and (D17), it is found that

$$k_B \frac{2K^2}{\zeta_2} \left[-C_{10} i J_1(i\zeta_2) + C_{11} H_1(i\zeta_2)\right]$$

$$= h_i \left[T_{g,e} - T_l - C_{10} J_o(i\zeta_2) - C_{11} i H_o(i\zeta_2)\right] \tag{D20}$$

The values of the integration constants C_{10} and C_{11} are now found by solving simultaneously equations (D19) and (D20). Insertion of these values in equation (D7) gives the desired equation for the temperature distribution through a trapezoidal section

$$\theta = \frac{\frac{h_i \zeta_2}{2K^2 k_B} (T_{g,e} - T_l) \left[H_1(i\zeta_1) J_o(i\zeta) + i J_1(i\zeta_1) i H_o(i\zeta)\right]}{\left[i J_1(i\zeta_1) H_1(i\zeta_2)\right] - \left[H_1(i\zeta_1) i J_1(i\zeta_2)\right] + \frac{h_i \zeta_2}{2K^2 k_B} \Gamma} \tag{20}$$

where

$$\Gamma = H_1(i\zeta_1) J_o(i\zeta_2) + i J_1(i\zeta_1) i H_o(i\zeta_2)$$

For a wedge, $\tau_1 \doteq 0$. Then, from equation (D15) it is seen that $\zeta_1 \doteq 0$, and as a consequence, $H_1(i\zeta_1) \doteq \infty$ and $i J_1(i\zeta_1) = 0$. Equation (20) then simplifies to

$$\theta = \frac{\frac{h_i \zeta_2}{2K^2 k_B} (T_{g,e}-T_l)\ J_o(i\zeta)}{\frac{h_i \zeta_2}{2K^2 k_B} J_o(i\zeta_2)-iJ_1(i\zeta_2)} \tag{21}$$

Concentric circle annulus approximation for blade leading edge. - The derivations of the equations giving blade temperatures at the inner and outer edges of the annular region are given as follows (fig. 4(c)):

$$\text{Heat entering from hot gas} = 2\pi \frac{D_o}{2} h_o(T_{g,e}-T_{B,o}) \tag{D21}$$

$$\text{Heat flowing over circle with diameter } D = 2\pi \frac{D}{2} k_B \frac{dT_B}{d\left(\frac{D}{2}\right)} \tag{D22}$$

$$\text{Heat leaving to coolant} = 2\pi \frac{D_i}{2} h_i(T_{B,i}-T_l) \tag{D23}$$

A solution of equation (D22) is

$$T_B = \left(\frac{Q}{2\pi k_B}\right) \log_e\left(C_{12} \frac{D}{2}\right) \tag{D24}$$

where C_{12} is an integration constant. Application of the boundary conditions

$$T_B = T_{B,o} \quad \text{when} \quad D = D_o$$

and

$$T_B = T_{B,i} \quad \text{when} \quad D = D_i$$

to equation (D24) results in the elimination of C_{12} and an evaluation of Q, namely,

$$T_{B,o}-T_{B,i} = \left(\frac{Q}{2\pi k_B}\right) \log_e\left(\frac{\frac{D_o}{2}}{\frac{D_i}{2}}\right)$$

or

$$Q = \frac{2\pi k_B \left(T_{B,o}-T_{B,i}\right)}{\log_e \frac{D_o}{D_i}} \tag{D25}$$

From simultaneous solutions of equations (D21), (D23), and (D25) it is found that

$$T_{B,o}-T_{B,i} = \frac{T_{g,e}-T_l}{1 + \frac{k_B}{\log_e \frac{D_o}{D_i}} \left(\frac{2}{D_o h_o} + \frac{2}{D_i h_i}\right)} \tag{25}$$

From a simultaneous solution of equation (D24) and equation (D24) with the inner boundary condition applied and use of equation (D25), it is found that

$$T_B = T_{B,i} + \frac{\log_e \frac{D}{D_i}}{\log_e \frac{D_o}{D_i}} \left(T_{B,o}-T_{B,i}\right) \tag{24}$$

From equations (D23) and (D25) and from equations (D21) and (D25) there are obtained

$$T_{B,i} = T_l + \frac{2k_B}{D_i h_i \log_e \frac{D_o}{D_i}} \left(T_{B,o}-T_{B,i}\right) \tag{22}$$

and

$$T_{B,o} = T_{g,e} - \frac{2k_B}{D_o h_o \log_e \frac{D_o}{D_i}} \left(T_{B,o}-T_{B,i}\right) \tag{23}$$

Equations (22) to (25) express the blade temperatures in terms of known quantities.

Section of blade approximated by parallel plates. - The derivation of the equations expressing the blade temperatures at the inner and outer edges of a blade section approximated by a region between parallel plates is given as follows (fig. 4(d)):

Q = heat entering from the hot gas = $h_o(T_{g,e}-T_{B,o})$

Q = heat leaving to the coolant = $h_i(T_{B,i}-T_l)$

Q = heat flowing through the section = $\frac{k_B}{\sigma}(T_{B,o}-T_{B,i})$

where σ is the distance between the plates. Equating these heat flows results in the following system of equations:

$$\frac{k_B}{\sigma}(T_{B,o}-T_{B,i}) = h_o(T_{g,e}-T_{B,o}) = h_i(T_{B,i}-T_l) \tag{D26}$$

A simultaneous solution of equations (D26) gives

$$T_{B,i} = \frac{T_l + \frac{k_B}{\sigma h_o h_i}(h_o T_{g,e}+h_i T_l)}{1 + \frac{k_B}{\sigma h_o h_i}(h_o+h_i)} \tag{26}$$

and

$$T_{B,o} = \frac{T_{g,e} + \frac{k_B}{\sigma h_o h_i}(h_o T_{g,e}+h_i T_l)}{1 + \frac{k_B}{\sigma h_o h_i}(h_o+h_i)} \tag{27}$$

From equations (26) and (27) it follows that

$$T_{B,o}-T_{B,i} = \frac{T_{g,e}-T_l}{1 + \frac{k_B}{\sigma h_o h_i}(h_o+h_i)} \tag{D27}$$

REFERENCES

1. Livingood, John N. B., and Brown, W. Byron: Analysis of Spanwise Temperature Distribution in Three Types of Air-Cooled Turbine Blade. NACA Rep. 994, 1950.

2. Brown, W. Byron, and Livingood, John N. B.: Cooling of Gas Turbines. III - Analysis of Rotor and Blade Temperatures in Liquid-Cooled Gas Turbines. NACA RM E7B11c, 1947.

3. Brown, W. Byron, and Monroe, William R.: Cooling of Gas Turbines. IV - Calculated Temperature Distribution in the Trailing Part of a Turbine Blade Using Direct Liquid Cooling. NACA RM E7B11d, 1947.

4. Jakob, Max: Heat Transfer. Vol. I. John Wiley & Sons, Inc., 1949.

5. Emmons, Howard W.: The Numerical Solution of Partial Differential Equations. Quart. Appl. Math., vol. II, no. 3, Oct. 1944, pp. 173-195.

6. McAdams, William H.: Heat Transmission. McGraw-Hill Book Co., Inc., 2d ed., 1942.

7. Byerly, William Elwood: An Elementary Treatise on Fourier's Series and Spherical, Cylindrical, and Ellipsoidal Harmonics. Ginn and Co., 1893.

8. Harper, D. R., 3d, and Brown, W. B.: Mathematical Equations for Heat Conduction in the Fins of Air-Cooled Engines. NACA Rep. 158, 1922.

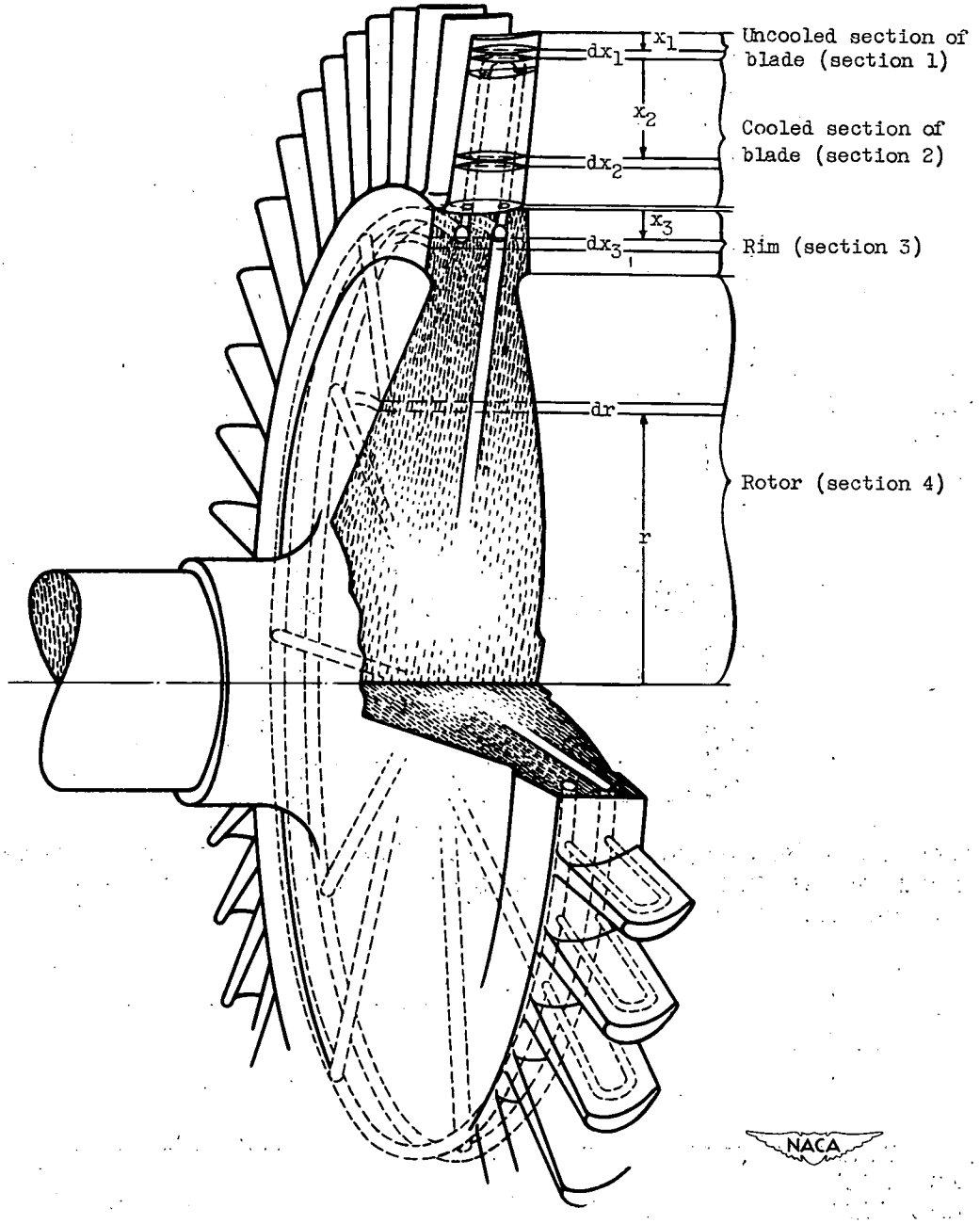

Figure 1. - Arrangement of internal-cooling passages in turbine.

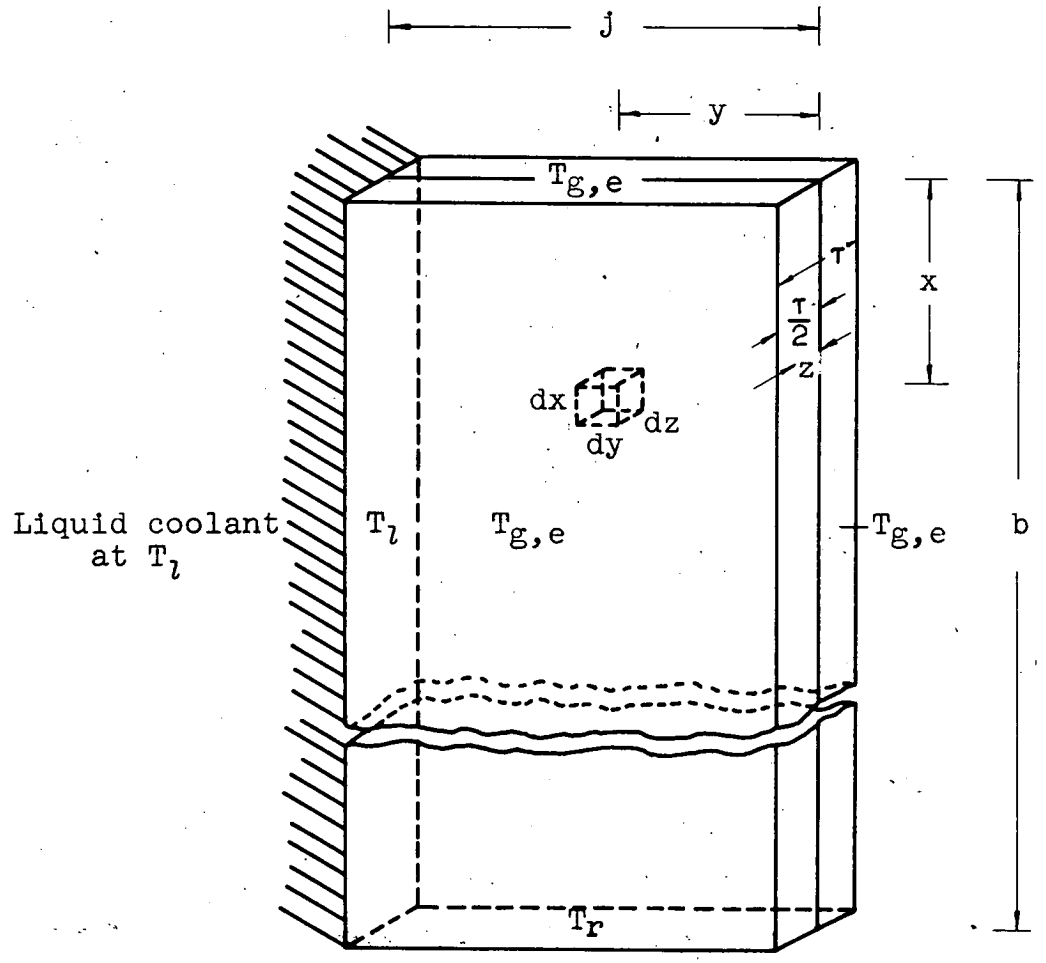

Figure 2. - Rectangular parallelepiped used to approximate trailing section of 4-inch turbine blade for three-dimensional analysis.

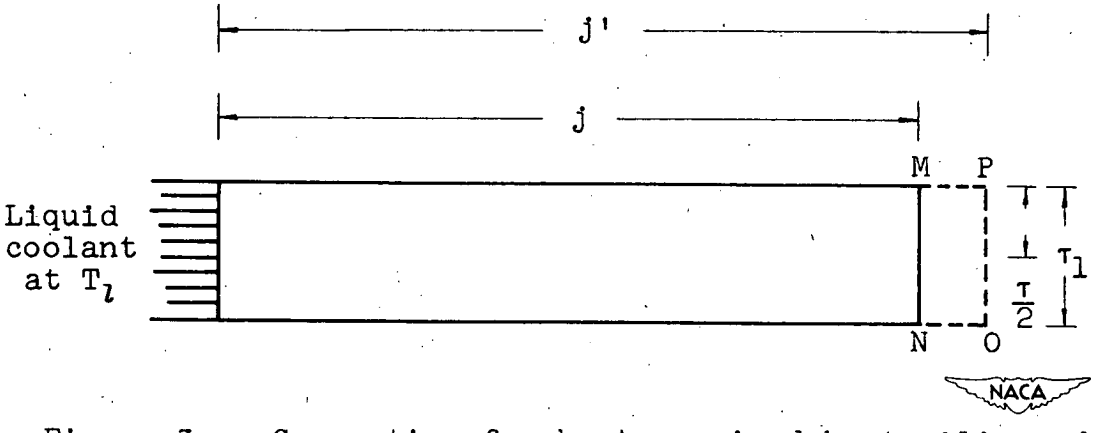

Figure 3. - Correction for heat received by trailing edge.

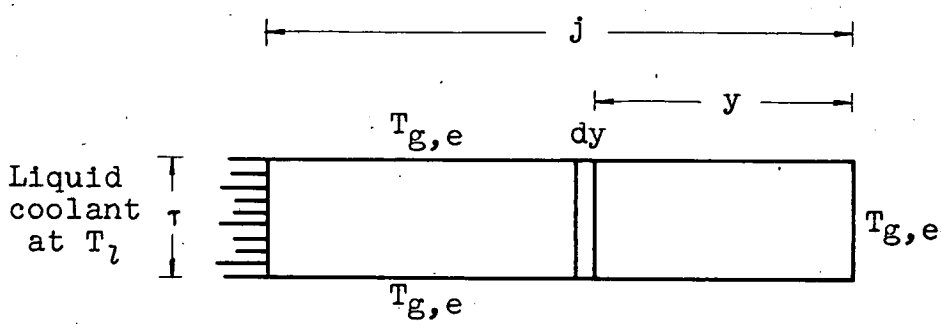

(a) Rectangle.

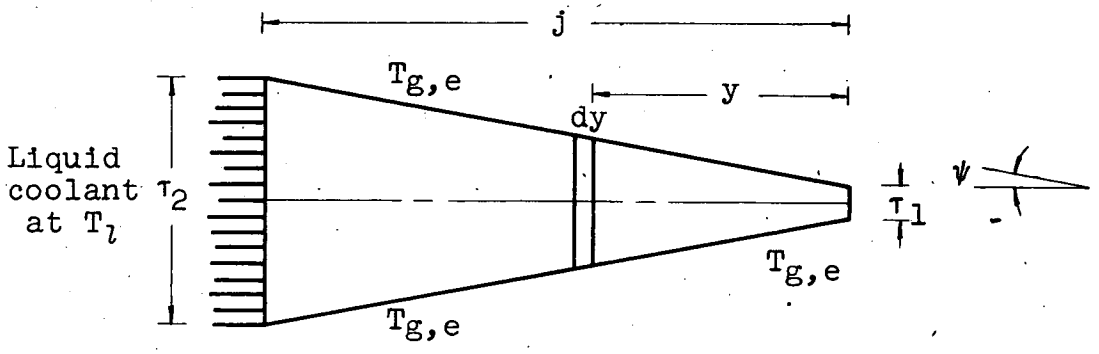

(b) Trapezoid.

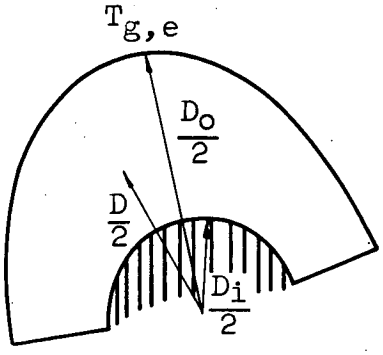

(c) Concentric circles.

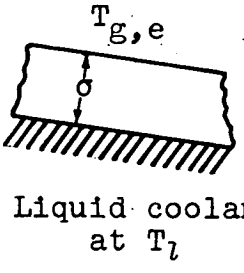

(d) Parallel plates.

Figure 4. - Simplified shapes used in one-dimensional chordwise analysis.

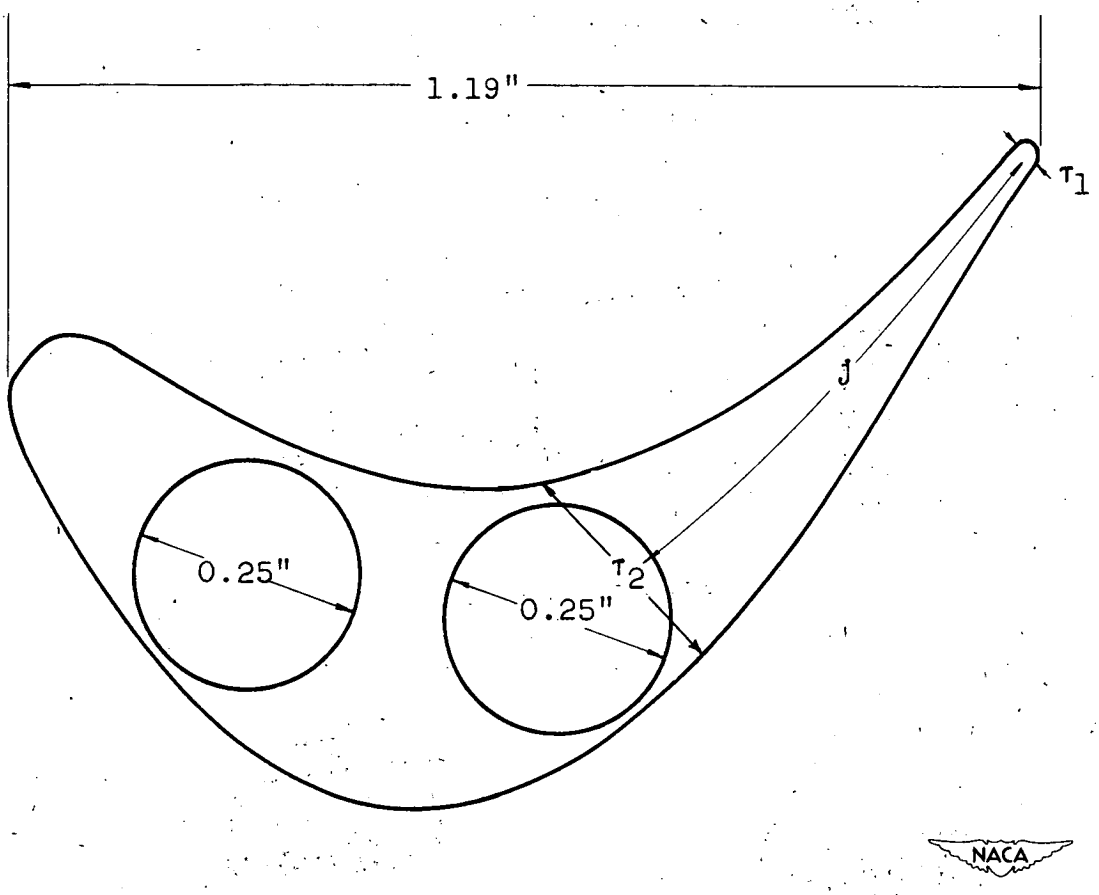

Figure 5. - Turbine-blade section showing coolant passages.

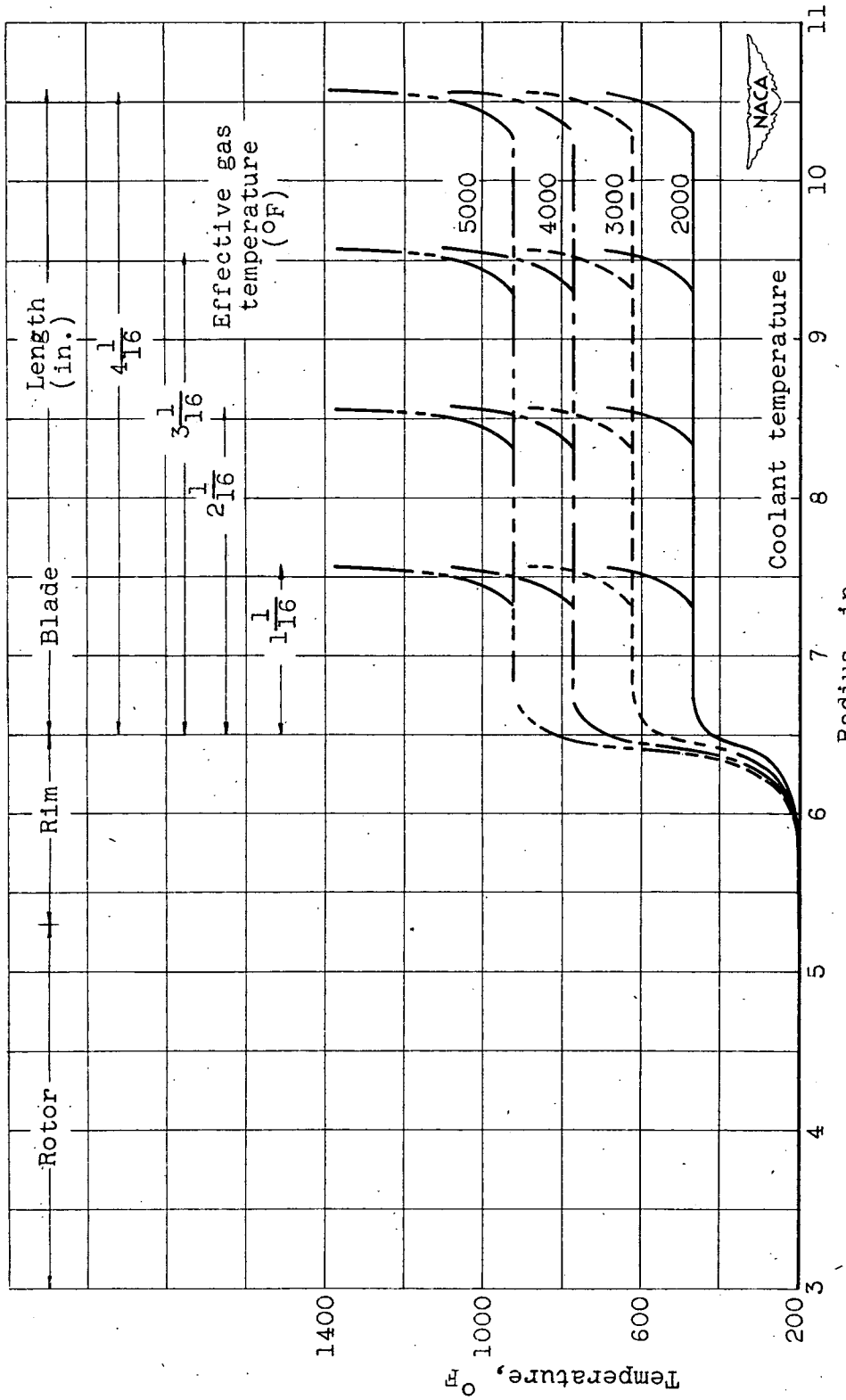

Figure 6. - Effect of various blade lengths on temperature distribution for water-cooled gas turbine for effective gas temperatures from 2000° to 5000° F. One-dimensional spanwise analysis. Coolant passages extend to within 1/16 inch of blade tip; coolant flow, 7 pounds per minute per blade; thermal conductivity of blade, 15 Btu/(hr)(ft)(°F).

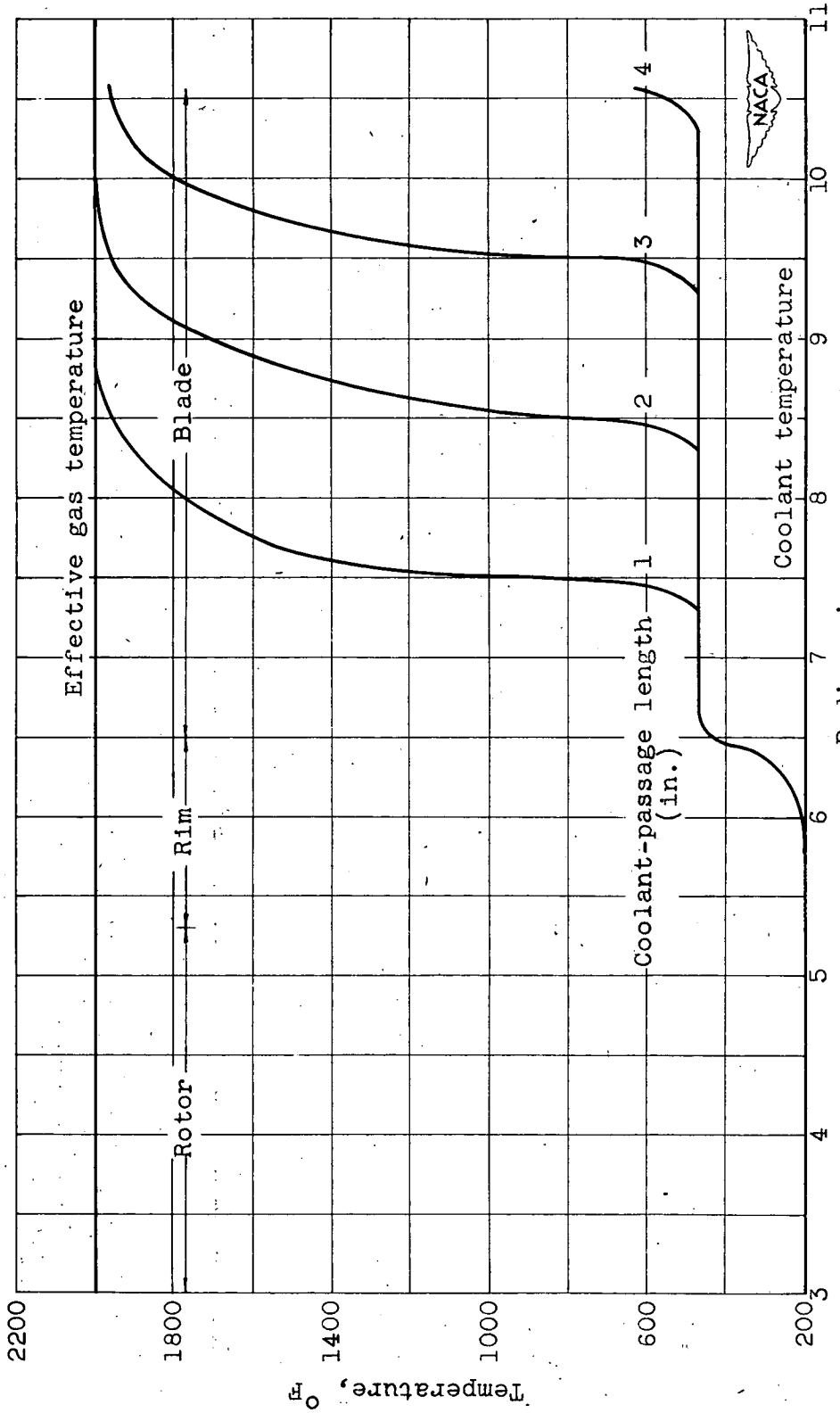

Figure 7. - Effect of various coolant-passage lengths on temperature distribution. One-dimensional spanwise analysis. Blade length, $4\frac{1}{16}$ inches; coolant flow, 7 pounds per minute per blade; thermal conductivity of blade, 15 Btu/(hr)(ft)(°F).

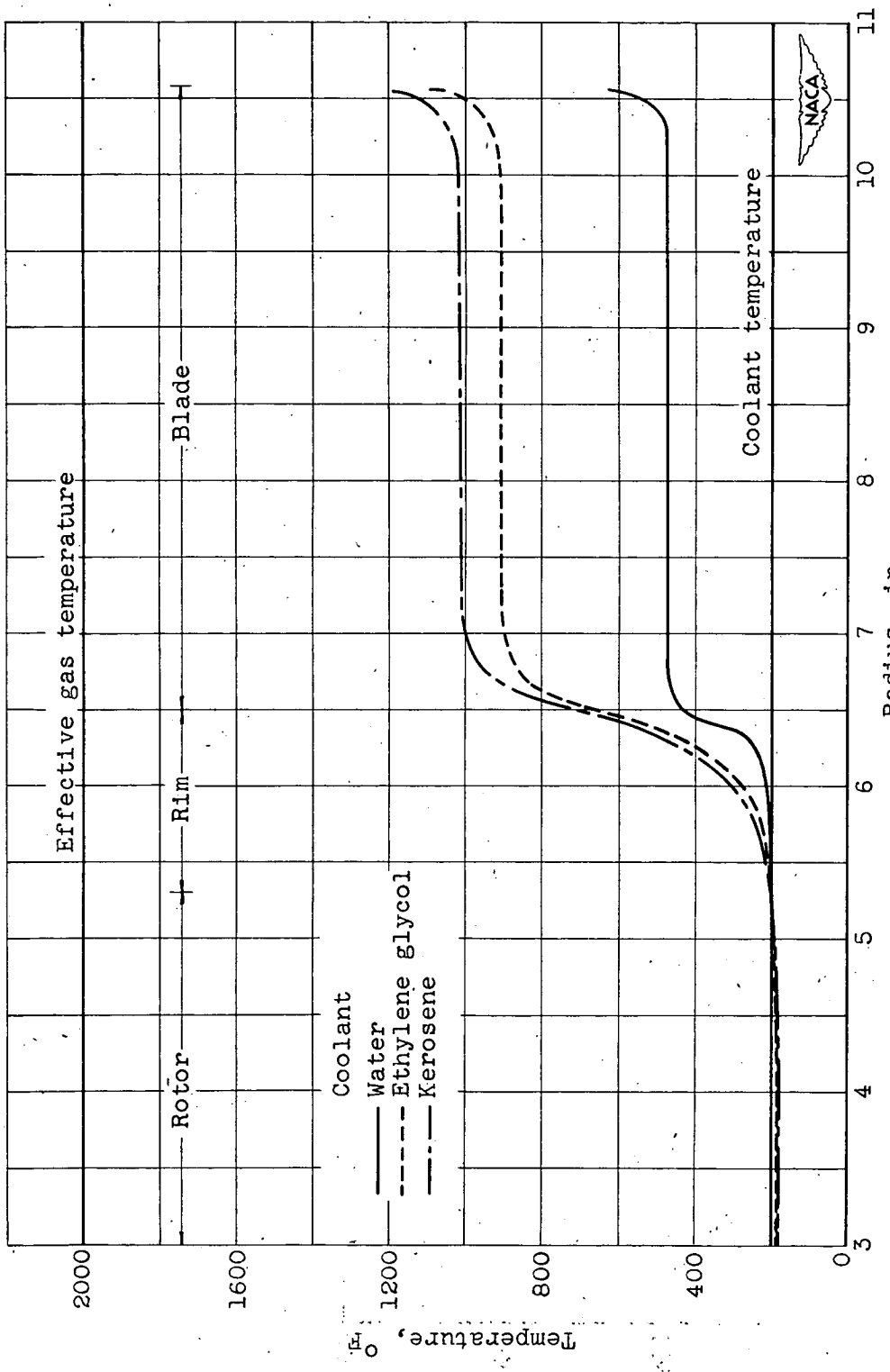

Figure 8. - Temperature distribution for gas turbine for various liquid coolants. One-dimensional spanwise analysis. Coolant-passage length, 4 inches; coolant passages extend to within 1/16 inch of blade tip; coolant flow, 7 pounds per minute per blade; thermal conductivity of blade, 15 Btu/(hr)(ft)(°F).

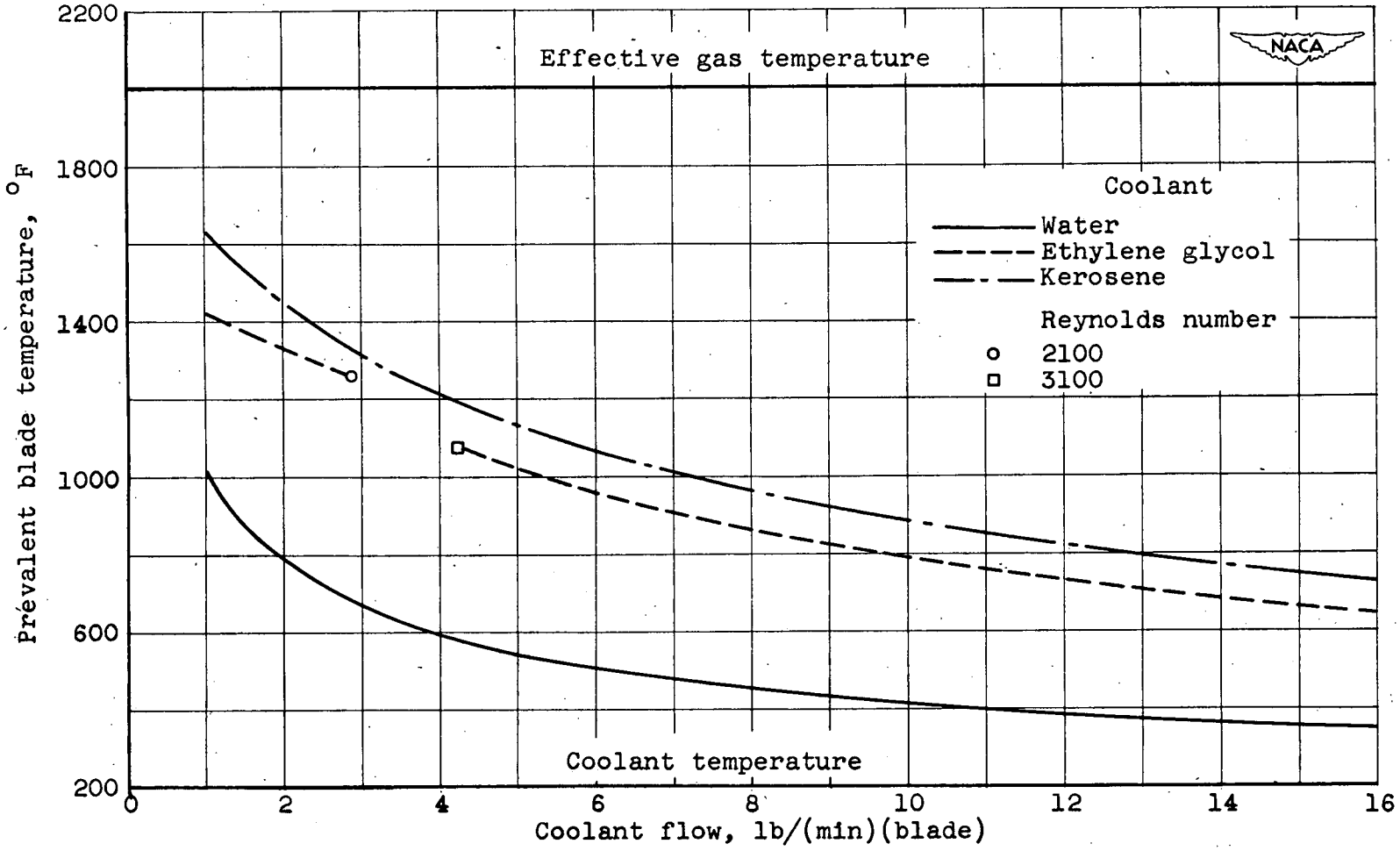

Figure 9. - Variation of prevalent blade temperature with coolant flow. One-dimensional spanwise analysis. Thermal conductivity of blade, 15 Btu/(hr)(ft)(°F).

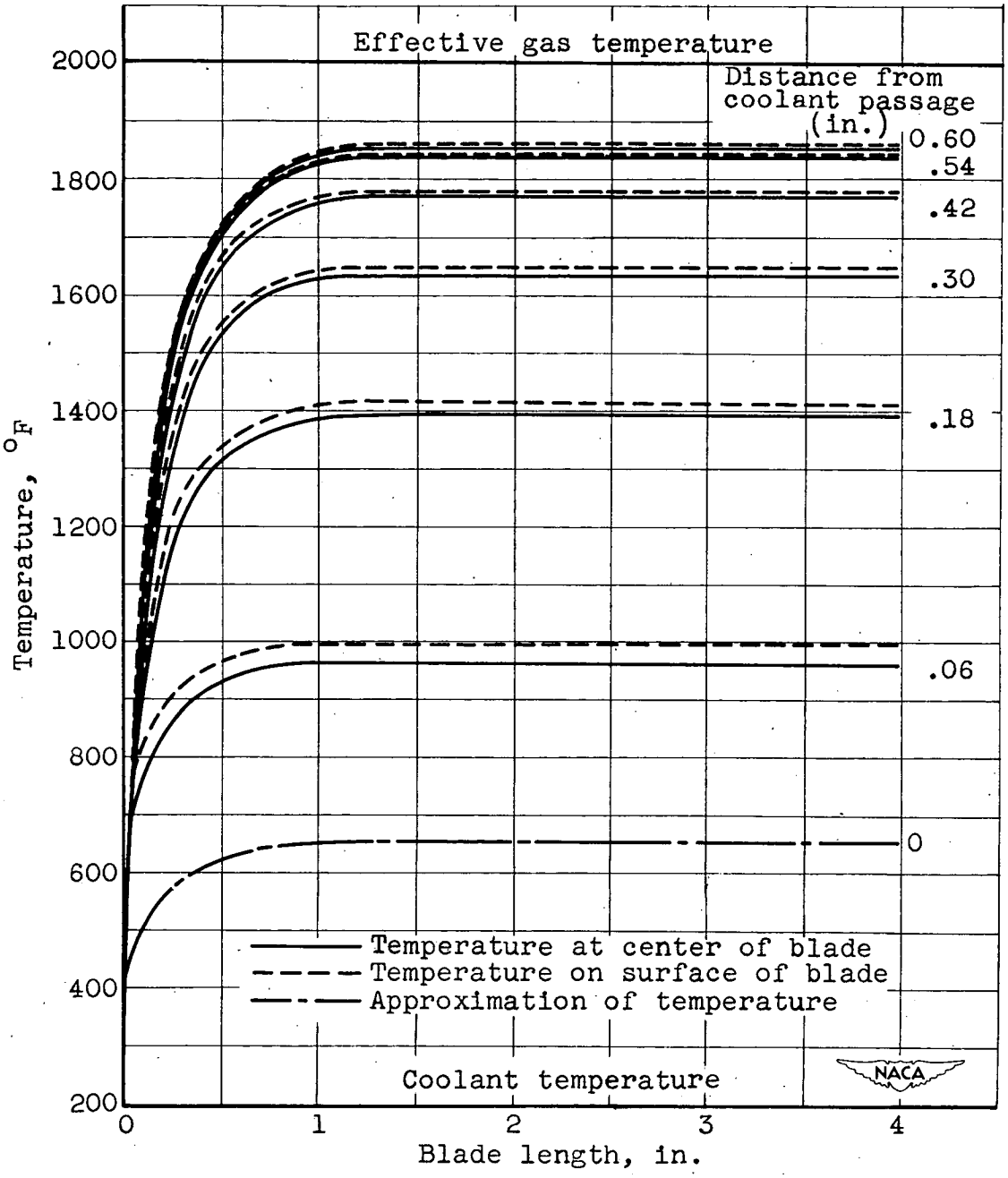

(a) Thermal conductivity of blade, 15 Btu/(hr)(ft)(°F).

Figure 10. - Three-dimensional temperature distribution in trailing section of turbine blade.

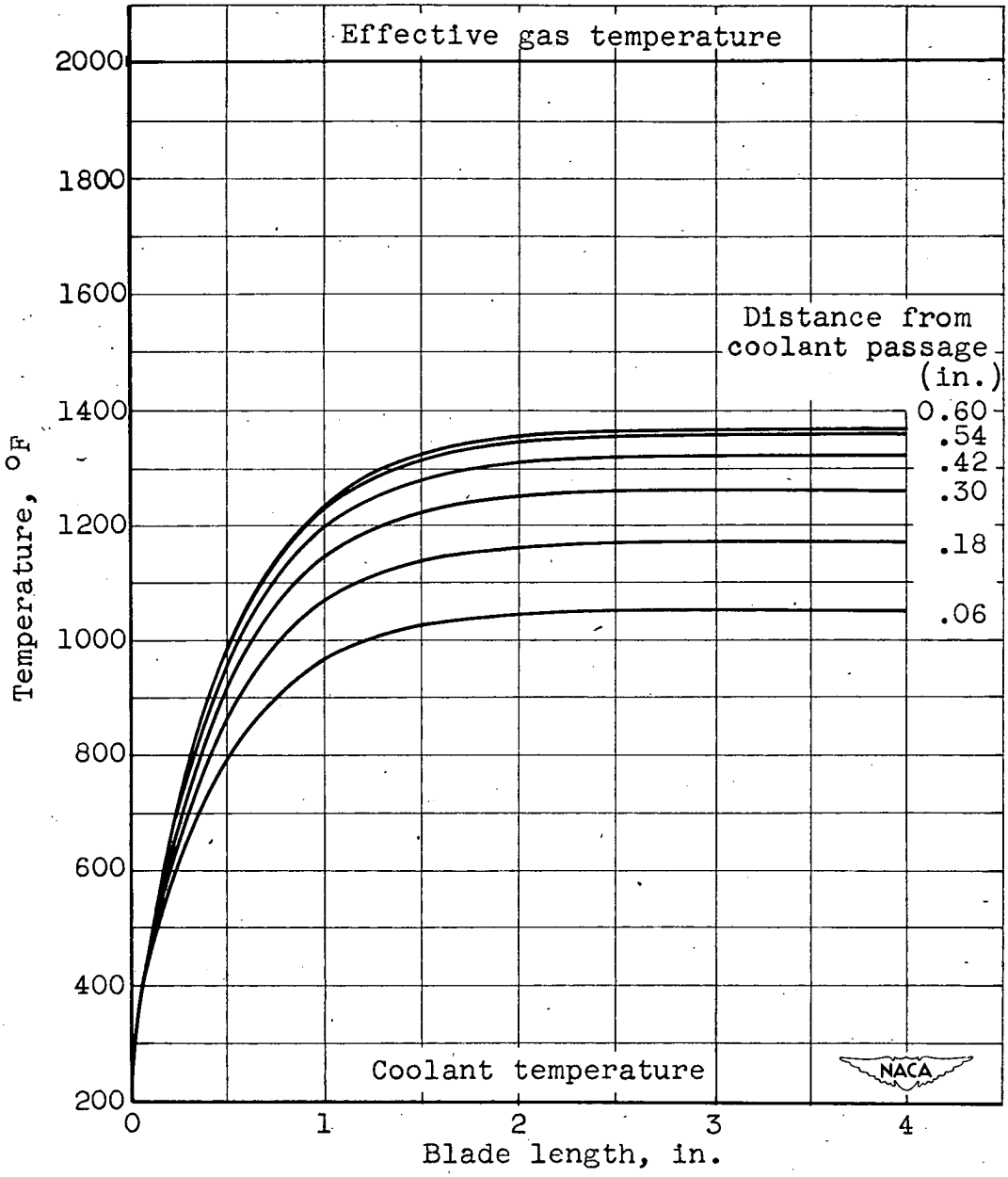

(b) Thermal conductivity of blade, 120 Btu/(hr)(ft)(°F).

Figure 10. - Continued. Three-dimensional temperature distribution in trailing section of turbine blade.

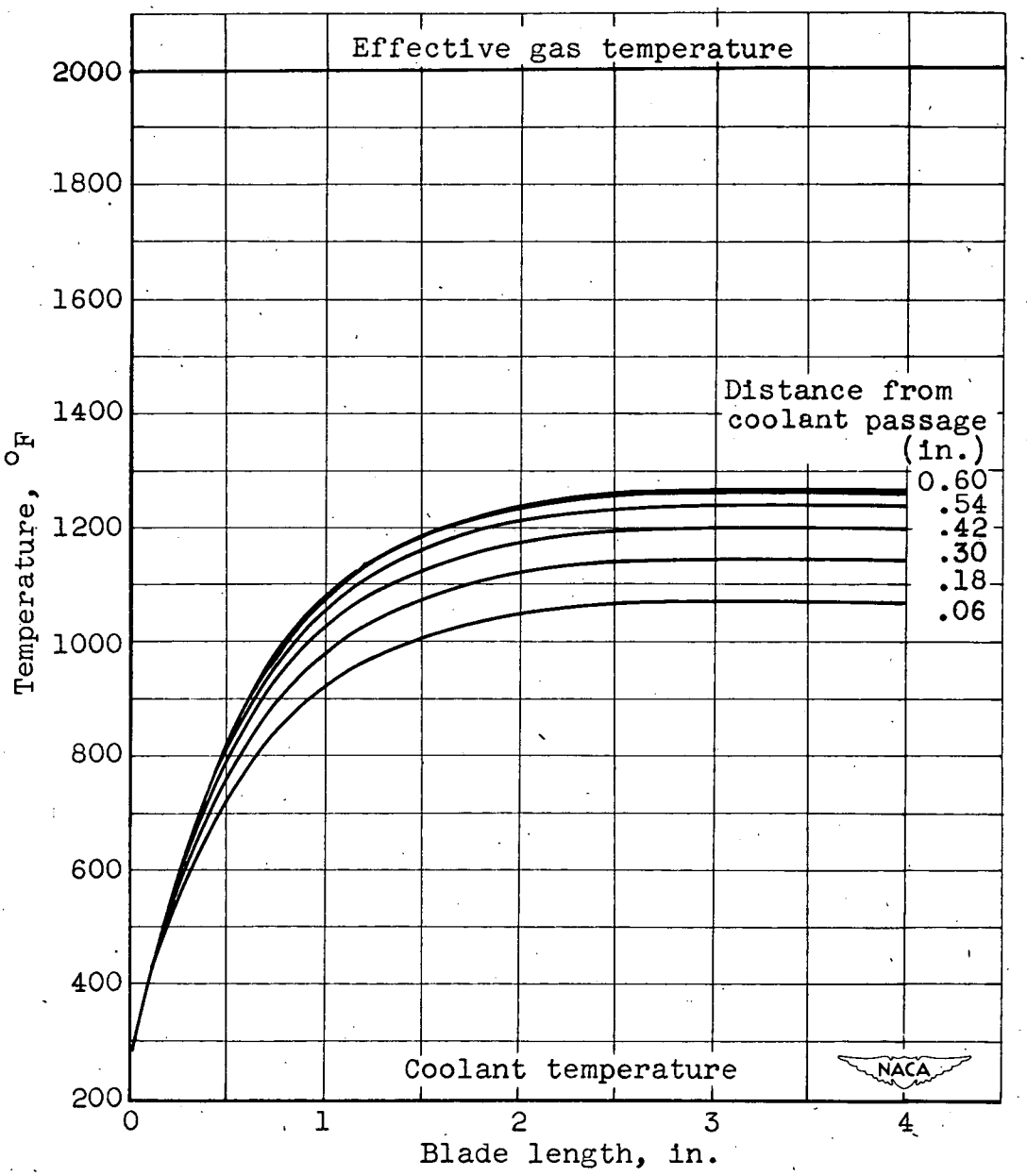

(c) Thermal conductivity of blade, 210 Btu/(hr)(ft)(°F).

Figure 10. - Concluded. Three-dimensional temperature distribution in trailing section of turbine blade.

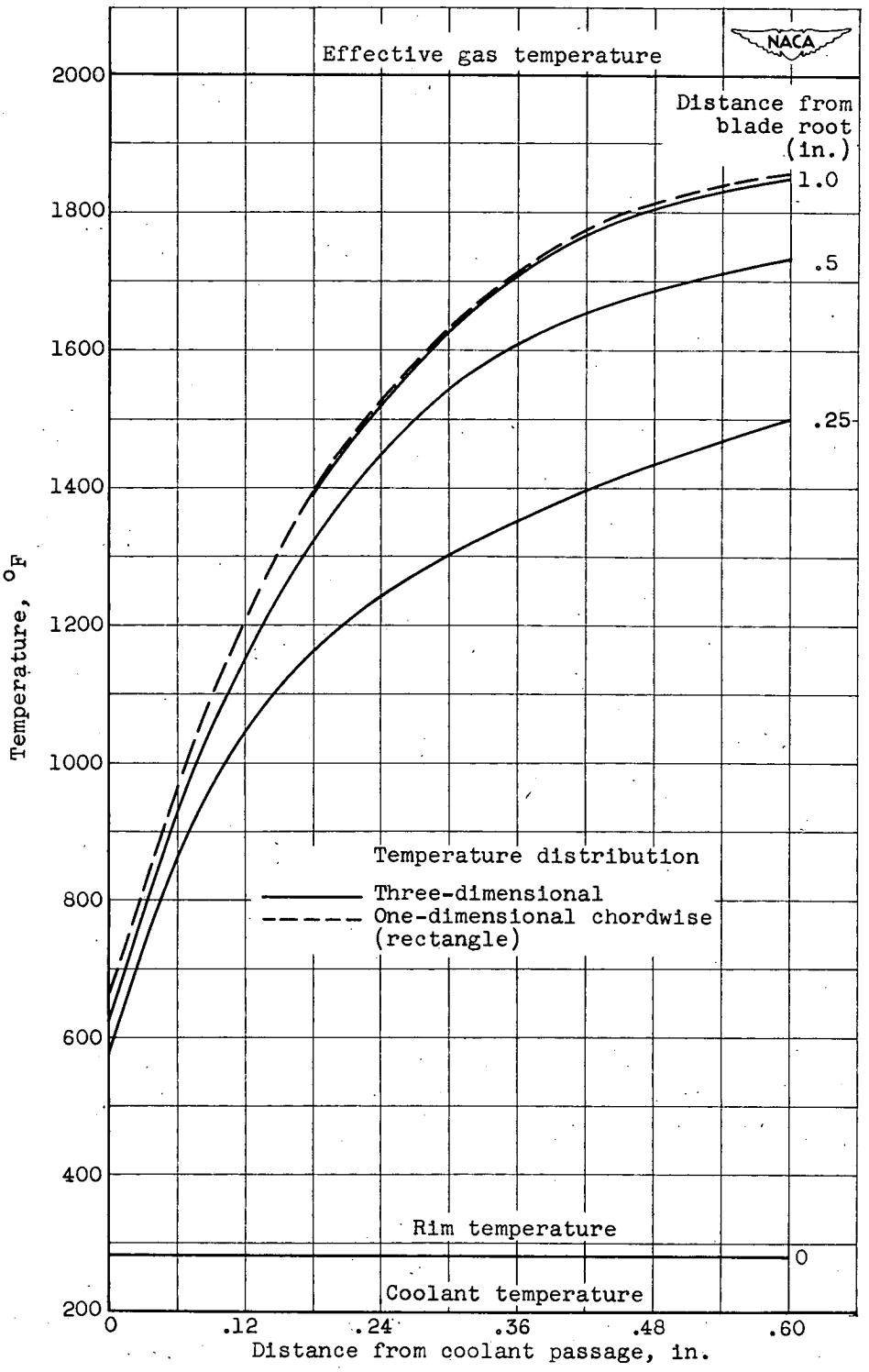

Figure 11. - Comparison of one-dimensional chordwise temperature distribution through rectangular trailing section with three-dimensional temperature distribution through rectangular parallelepiped. Thermal conductivity of blade, 15 Btu/(hr)(ft)(°F).

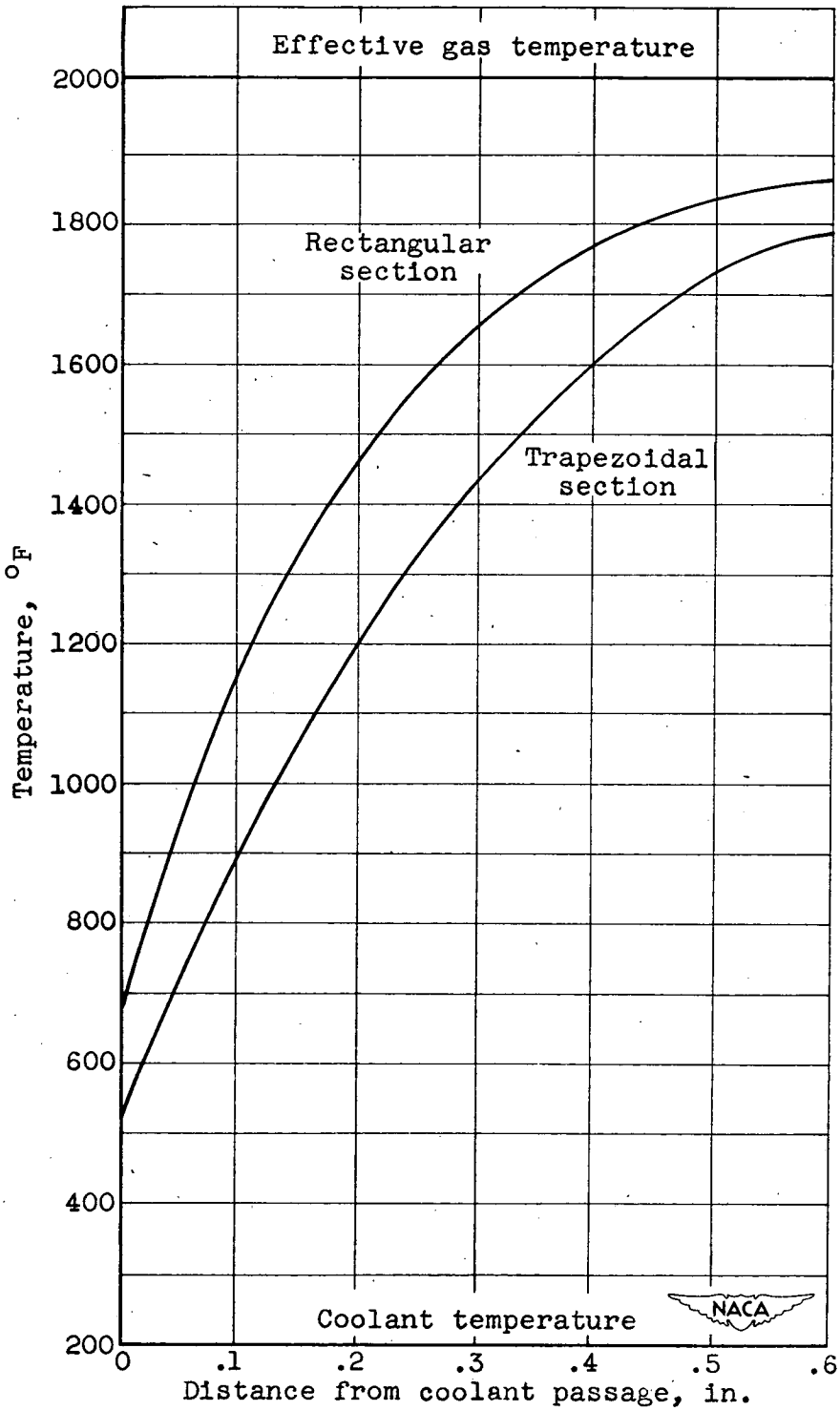

Figure 12. - One-dimensional chordwise analysis of effect of shape on prevalent blade temperature. Thermal conductivity of blade, 15 Btu/(hr)(ft)(°F).

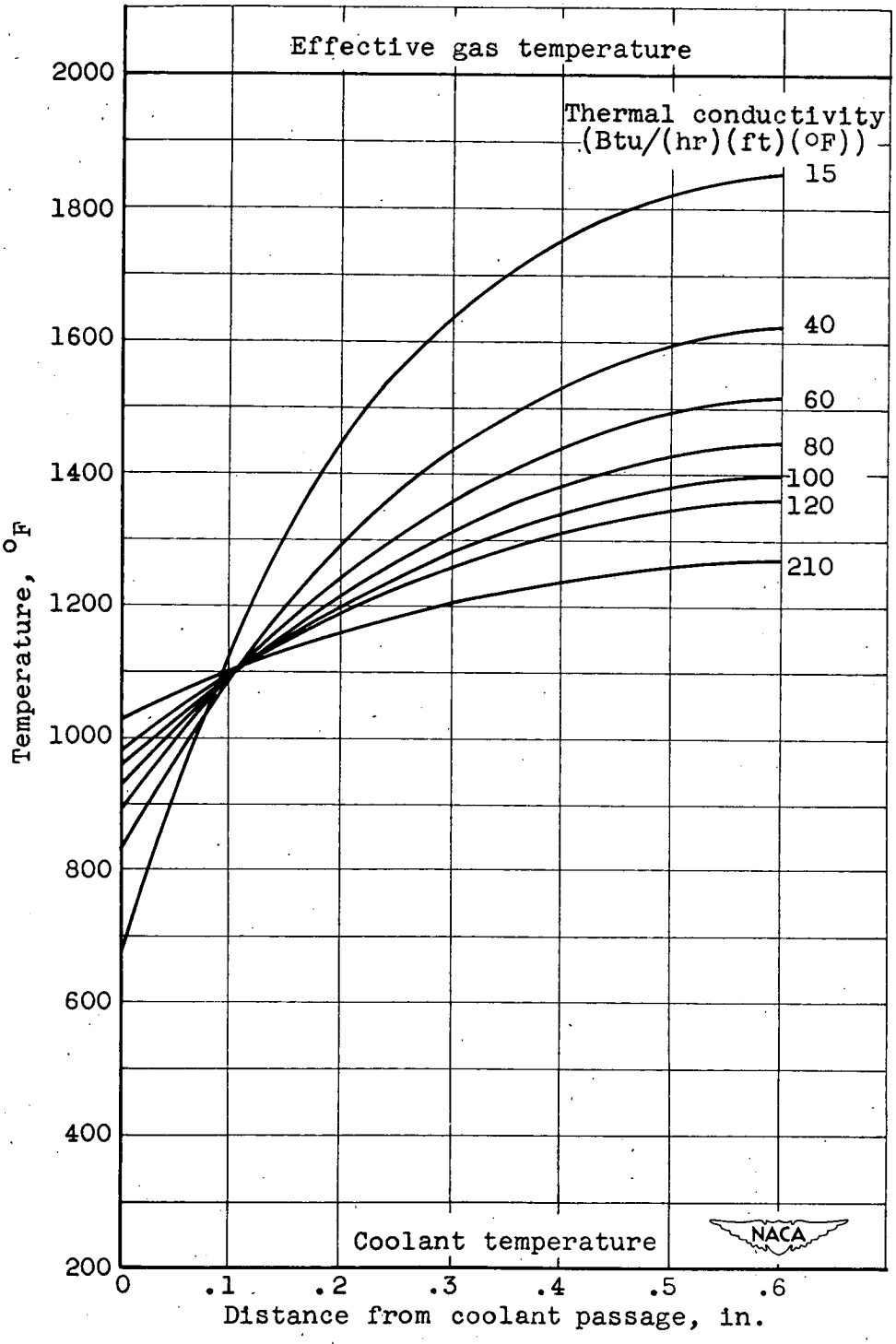

(a) Rectangular trailing section.

Figure 13. - One-dimensional chordwise analysis of prevalent blade temperature for trailing section of blade.

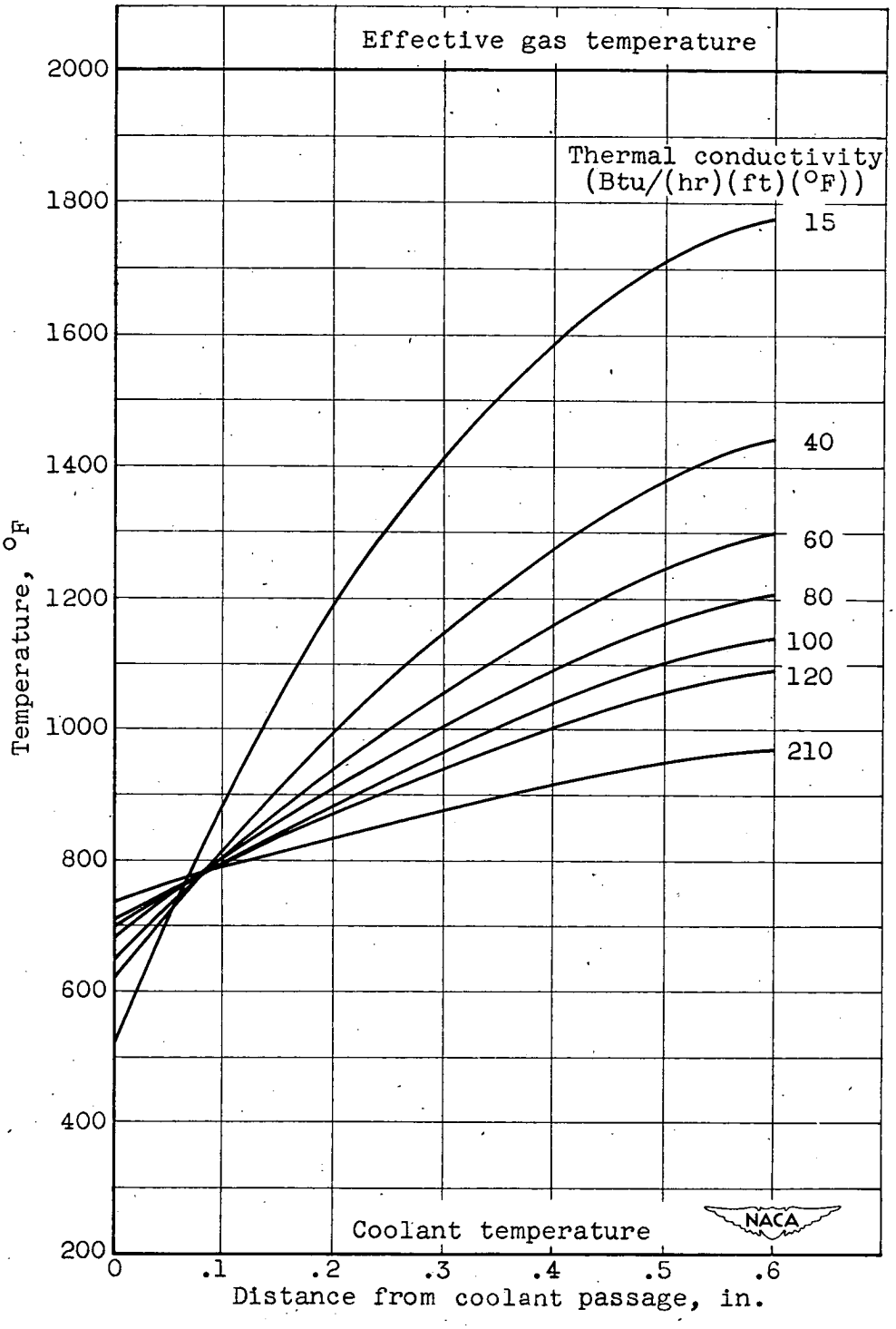

(b) Trapezoidal trailing section.

Figure 13. - Concluded. One-dimensional chordwise analysis of prevalent blade temperature for trailing section of blade.

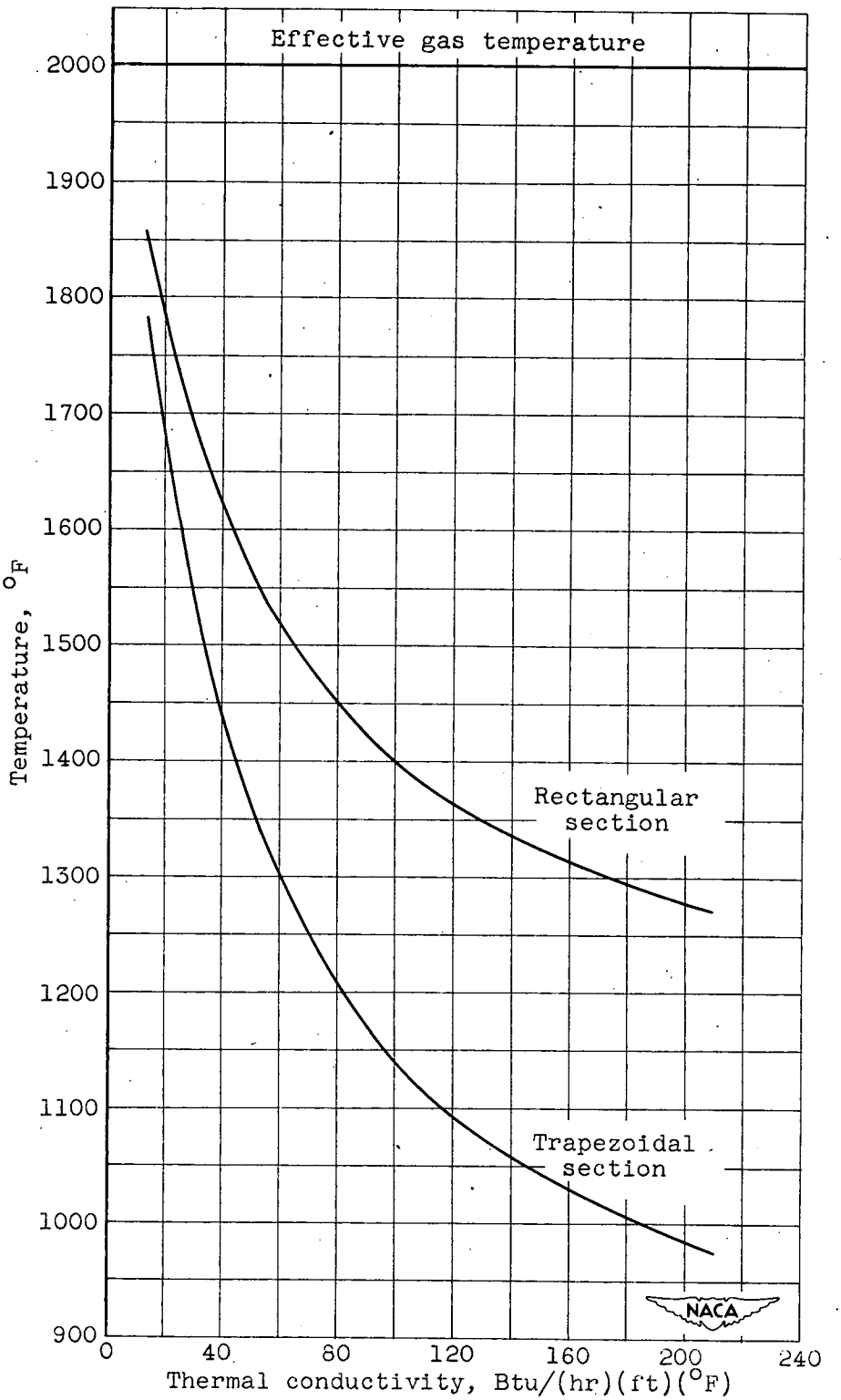

Figure 14. - Trailing-edge temperatures obtained from one-dimensional chordwise analysis. Coolant temperature, 200° F.

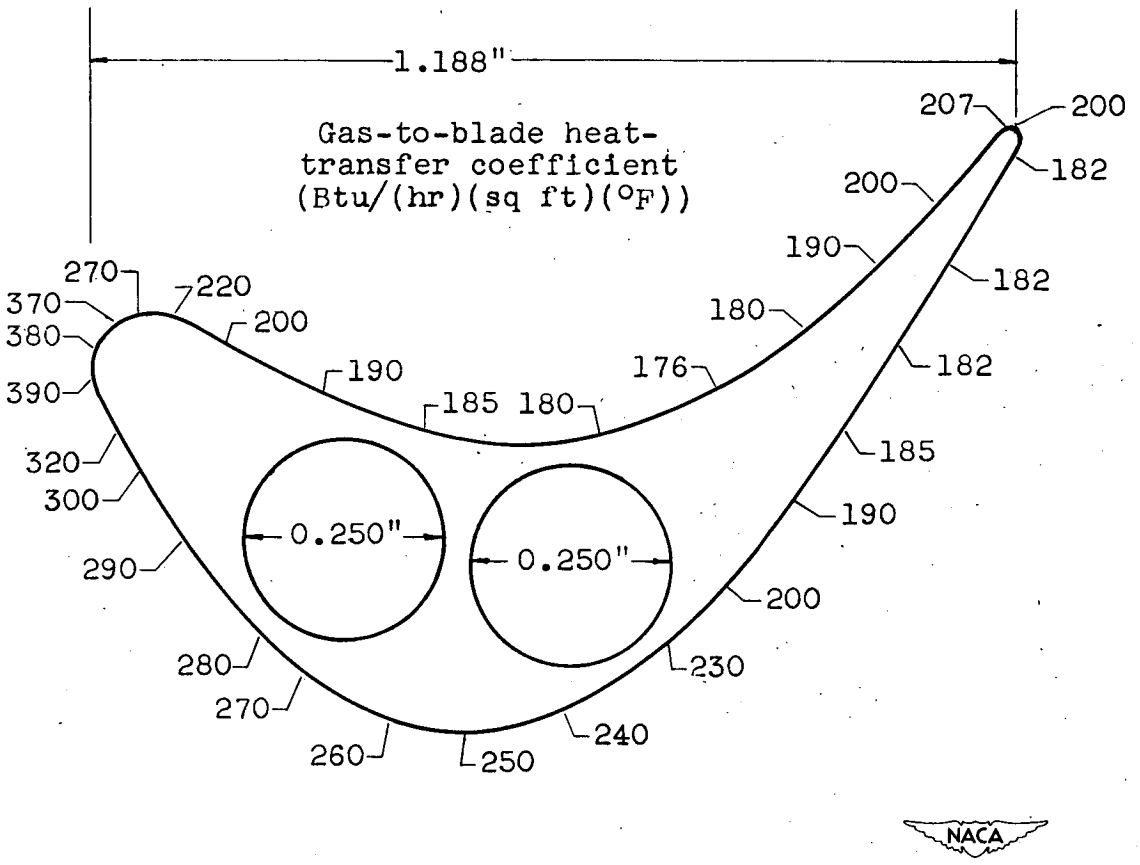

Figure 15. - Cross section of turbine blade showing typical variation of heat-transfer coefficient around blade perimeter.

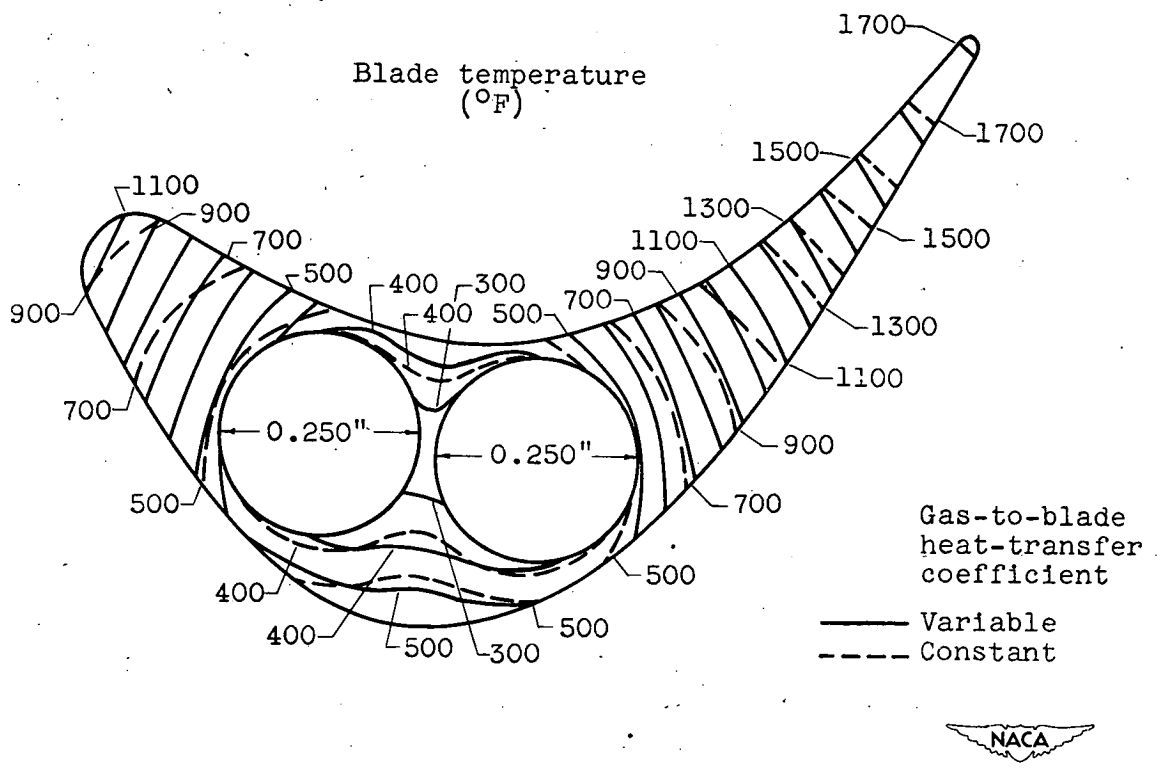

Figure 16. - Effect of variation of gas-to-blade heat-transfer coefficient on temperature distribution through cross section of water-cooled turbine blade. Thermal conductivity of blade, 15 Btu/(hr)(ft)(°F); effective gas temperature, 2000° F; average water temperature, 200° F.

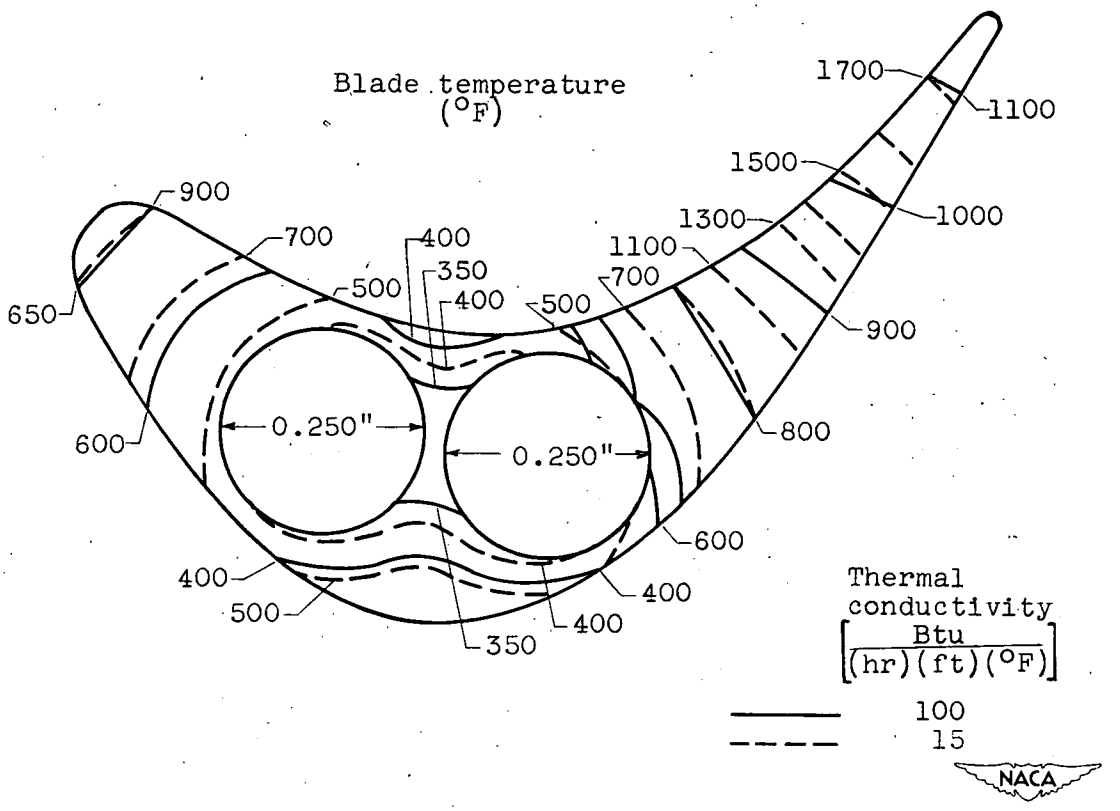

Figure 17. - Effect of variation of thermal conductivity on temperature distribution through water-cooled turbine blade. Gas-to-blade heat-transfer coefficient, 222 Btu/(hr)(sq ft)(°F); effective gas temperature, 2000° F; average water temperature, 200° F.

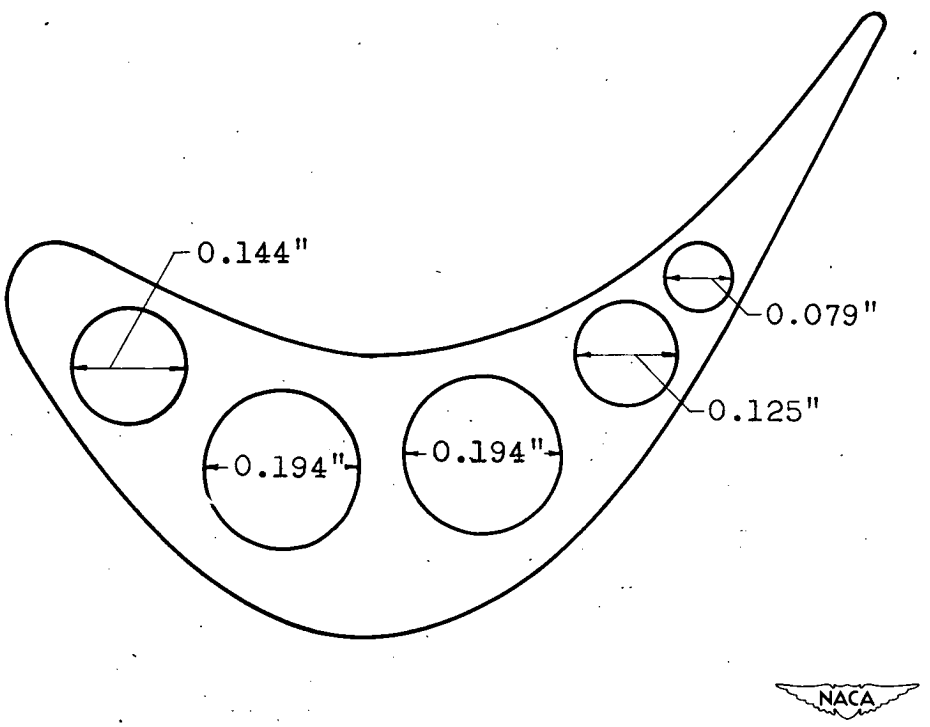

Figure 18. - Cross section of water-cooled turbine blade showing location and size of five coolant passages used in determination of effect of varying trailing-section length on trailing-edge temperature.

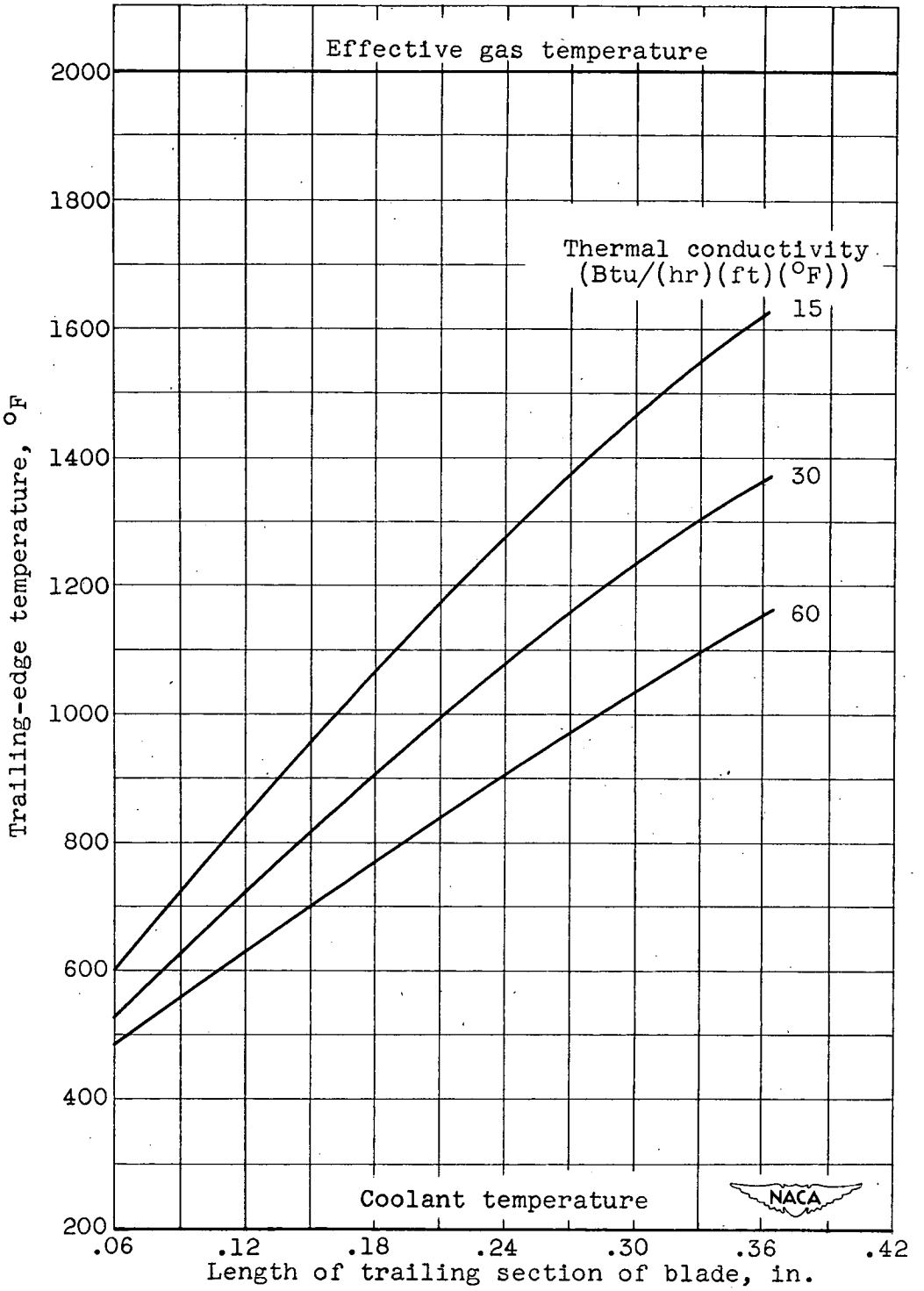

Figure 19. - Trailing-edge temperature as function of length of trailing section of blade for water-cooled turbine blades with five coolant passages and various thermal conductivities.

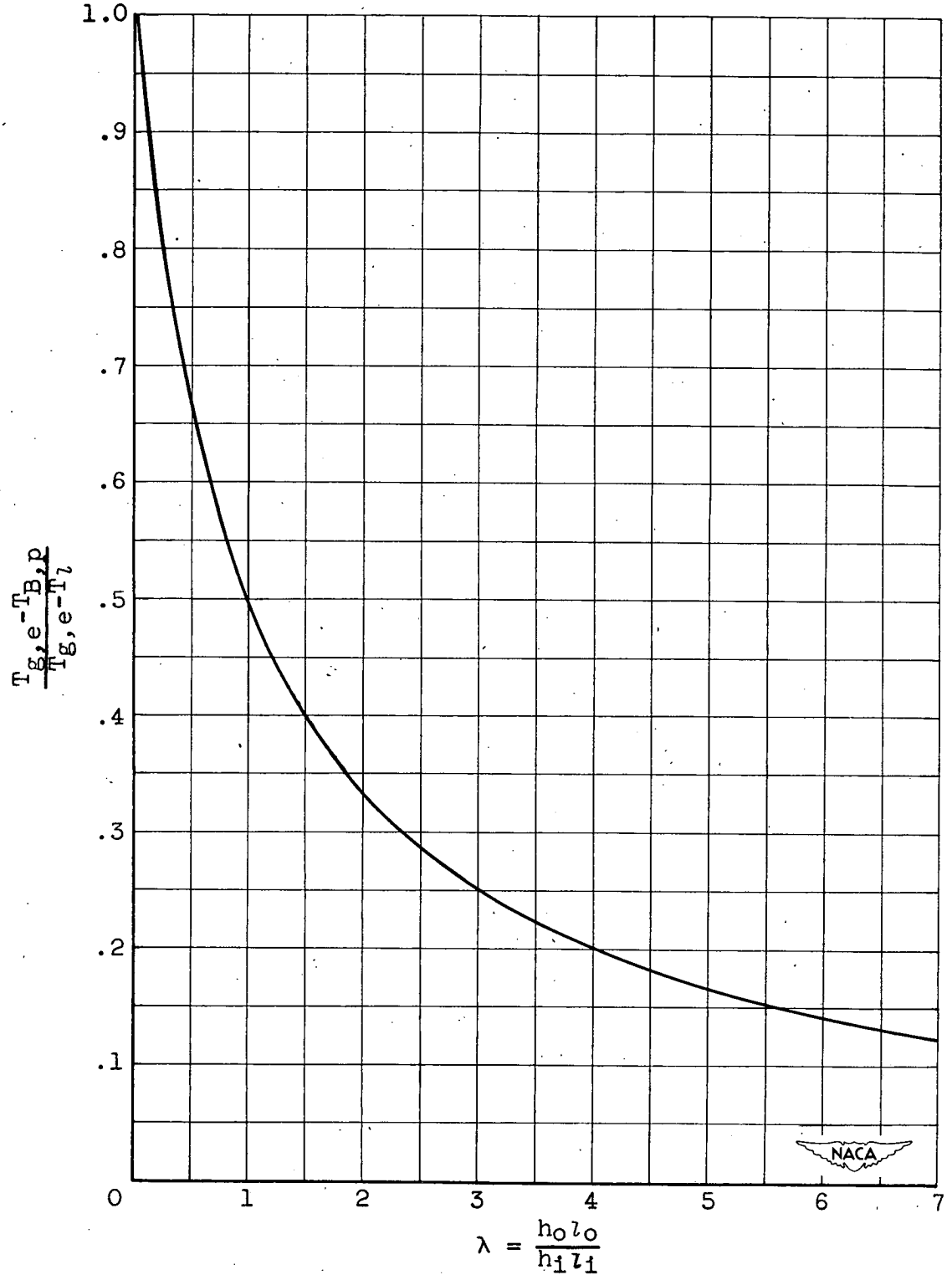

Figure 20. - Nondimensional chart for use in determination of prevalent blade temperature.

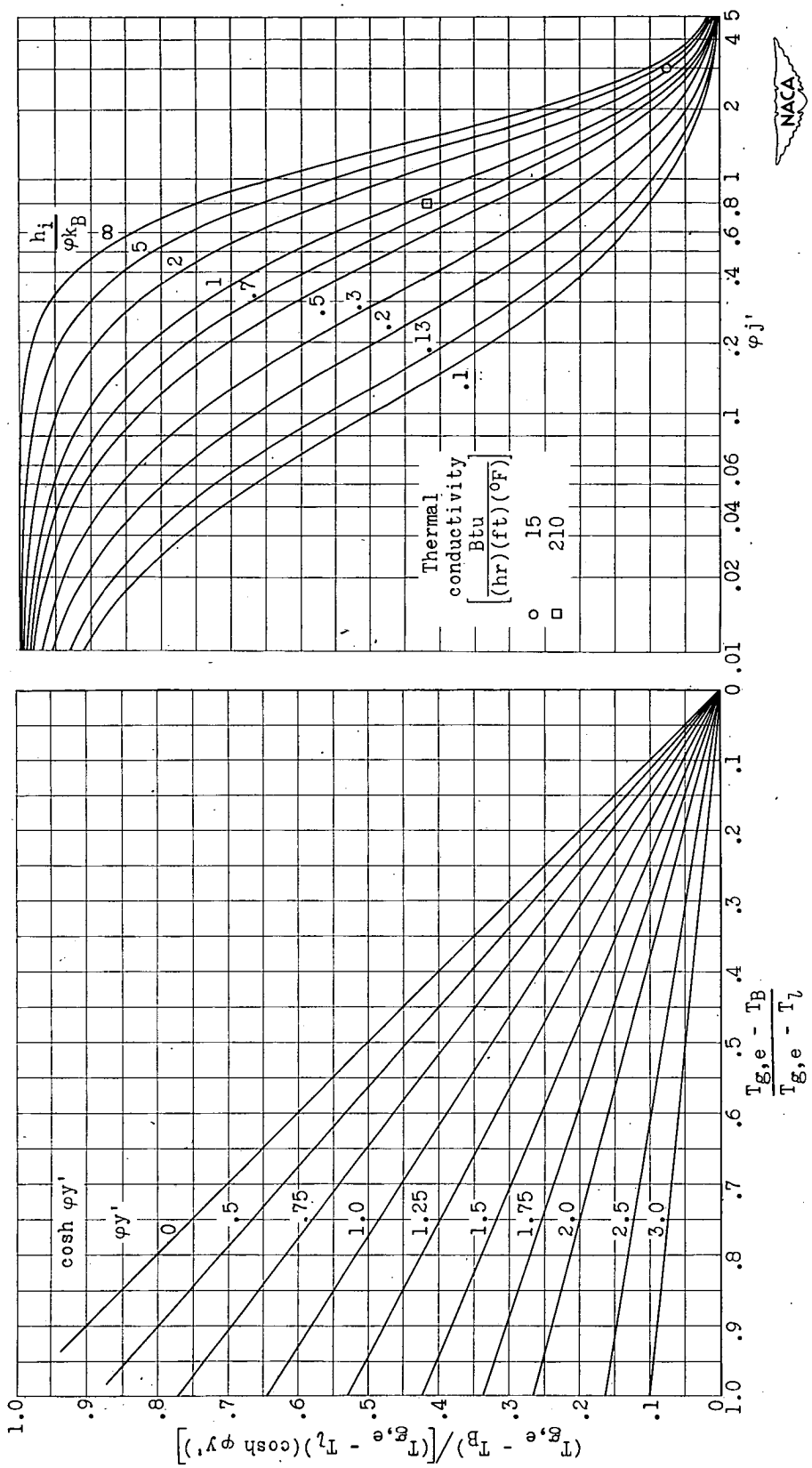

Figure 21. - Nondimensional chart for use in determination of temperature distribution through rectangular trailing section of cooled turbine blade.

Abstract

Analytical methods are presented for computing temperature distributions in liquid-cooled turbine blades or in simplified shapes used to approximate sections of liquid-cooled turbine blades. Nondimensional charts are presented for use in the simplification of some of the calculations. Illustrative examples are also included to demonstrate the use of the various equations and nondimensional charts and to show trends of the various temperature distributions.

One-dimensional spanwise temperature distributions gave satisfactory results near the coolant passages. One-dimensional chordwise distribution gave a good first approximation to the actual solution in cases where rim cooling was insignificant.

Abstract

Analytical methods are presented for computing temperature distributions in liquid-cooled turbine blades or in simplified shapes used to approximate sections of liquid-cooled turbine blades. Nondimensional charts are presented for use in the simplification of some of the calculations. Illustrative examples are also included to demonstrate the use of the various equations and nondimensional charts and to show trends of the various temperature distributions.

One-dimensional spanwise temperature distributions gave satisfactory results near the coolant passages. One-dimensional chordwise distribution gave a good first approximation to the actual solution in cases where rim cooling was insignificant.

Abstract

Analytical methods are presented for computing temperature distributions in liquid-cooled turbine blades or in simplified shapes used to approximate sections of liquid-cooled turbine blades. Nondimensional charts are presented for use in the simplification of some of the calculations. Illustrative examples are also included to demonstrate the use of the various equations and nondimensional charts and to show trends of the various temperature distributions.

One-dimensional spanwise temperature distributions gave satisfactory results near the coolant passages. One-dimensional chordwise distribution gave a good first approximation to the actual solution in cases where rim cooling was insignificant.

Heat Transfer 1.1.4.2

NACA

Analysis of Temperature Distribution in Liquid-Cooled Turbine Blades.

By John N. B. Livingood and W. Byron Brown

NACA TN 2321

April 1951

(Abstract on Reverse Side)

Turbine Cooling 3.7.2

NACA

Analysis of Temperature Distribution in Liquid-Cooled Turbine Blades.

By John N. B. Livingood and W. Byron Brown

NACA TN 2321

April 1951

(Abstract on Reverse Side)

Livingood, John N. B., and Brown, W. Byron

NACA

Analysis of Temperature Distribution in Liquid-Cooled Turbine Blades.

By John N. B. Livingood and W. Byron Brown

NACA TN 2321

April 1951

(Abstract on Reverse Side)

NACA